MULTICOMPONENT POLYMER NANOCOMPOSITES: CHARACTERIZATION OF INTERFACIAL INTERACTIONS AND THEIR EFFECTS ON BULK PROPERTIES

A Dissertation

Presented to the Faculty of the Graduate School

of Cornell University

in Partial Fulfillment of the Requirements for the Degree of

Doctor of Philosophy

by

Loan Thanh Vo

February 2010

MULTICOMPONENT POLYMER NANOCOMPOSITES:
CHARACTERIZATION OF INTERFACIAL INTERACTIONS AND THEIR EFFECTS ON BULK PROPERTIES

Loan Thanh Vo, Ph.D.
Cornell University 2010

Polymer blending and copolymerization provide techniques to engineer polymeric materials with desired properties. Inorganic particles may also be added to the polymers to further enhance mechanical properties. In particular, clay nanoparticles, with their large surface area per unit weight, can both reinforce polymers and change polymer structure. In copolymers and polymer blends, nanoparticles can suppress crystallinity and stabilize domain morphology. This thesis details the effects of clay nanoparticles on multicomponent polymer systems.

The first part of the thesis focuses on butadiene-styrene copolymer interactions with clay nanoparticles and the effect of those interactions on the kinetics of copolymer intercalation. Dielectric relaxation spectroscopy was used to measure interfacial polymer relaxations which are a measure of interaction strength. Copolymers of different compositions were studied, and the copolymers with higher styrene concentration had slower polymer dynamics. Dielectric spectroscopy results were compared to the intercalation kinetics measured with xray diffraction. Copolymers with higher styrene concentration intercalated the clay nanoparticles faster indicating that there is a correlation between strong copolymer interactions and fast intercalation kinetics.

The second part of the thesis focuses on characterizing various polymer

blend nanocomposites to determine what variables control blend morphology and properties. Both thermodynamic variables (such as polymer-polymer and polymer-clay interactions) and kinetic variables (such as viscosities of the matrix and domain phases) control domain size. To stabilize the domain morphology in blend nanocomposites and improve the mechanical properties, clay nanoparticles need to interact favorably with both polymers to reduce the interfacial tension. To reduce domain size, the nanoparticles should also change the viscosities of the domain and matrix phases so that they are comparable.

BIOGRAPHICAL SKETCH

Loan Thanh Vo was born on January 16, 1982 in Tulsa, OK. She graduated from Booker T. Washington High School in the year 2000 with a International Baccalaureate diploma and continued her schooling at the University of Tulsa. During her undergraduate years, she completed two years of undergraduate research at the University of Tulsa, participated in Research Experience for Undergraduates at Harvey Mudd College, and interned two summers at IBM Almaden under the American Physical Society undergraduate summer fellowship award. She received her Bachelor of Science degree in Chemistry in 2004. That same year she was awarded the National Science Foundation Graduate Research fellowship and began her graduate studies in the Materials Science and Engineering department at Cornell University.

ACKNOWLEDGEMENTS

I would like to thank Emmanuel Giannelis for his advice and encouragement and for giving me the freedom to learn how to make decisions in research and communicate my ideas. I would like to acknowledge Suren Hayrapetyan, Alexandre Vermogen, and Haris Retsos for their guidance in various projects throughout my studies at Cornell. Antonios Kelarakis, Robert Rodriguez, and Lou Estevez have also contributed to my work, and I am appreciative of their efforts. I am grateful for insightful discussions with Rich Vaia and Anastasiadis Spiros and camaraderie with fellow students and group members. Finally, I would like to thank my parents, Luan and Kim Vo, for their hard work and sacrifices, and my husband, Creighton Thomas for his support and inspiration.

TABLE OF CONTENTS

LIST OF TABLES

LIST OF FIGURES

CHAPTER 1

INTRODUCTION

Nanotechnology, the study of manipulating structures smaller than 100nm, has transformed how materials are designed and used. Ever since Richard Feynman declared back in 1959 that "there's plenty of room at the bottom," researchers have been creating and characterizing materials with structures with smaller and smaller features. In that time, polymer science has progressed to nanosized polymeric structures (such as domains in phase separated polymer blends and block copolymers) and then expanded to hybrid polymeric materials with both nanosized polymer structures and inorganic components (such as clay nanoparticles). This thesis presents nanocomposites of multicomponent polymer systems with clay nanoparticles. The interactions among the many nanosized components in the composites are studied in an effort to understand the material properties and to create a material with the desired properties.

1.1 Polymer-clay nanocomposites

Research on polymer-clay nanocomposites over the past two decades has revealed materials that have better properties than neat polymers or the polymers with traditional fillers. Polymer-clay nanocomposites are stiffer than both neat polymers [1] and polymers with the same weight percent traditional filler [2]. Polymer-clay nanocomposites have a lower coefficient of thermal expansion (CTE) than neat polymers [3], and clay nanoparticles are more efficient at reducing CTE compared to traditional talc filler [4]. Clay nanoparticles decrease the gas permeability [5, 6, 7] and flammability [8, 9] of polymers. Polymer-clay nanocomposites are also more thermally stable than neat polymers [9, 10].

Clay nanoparticles are comprised of stacked silicate sheets that are 1nm thick. The lateral dimensions of the layers vary from 30nm to several micrometers. They can be combined with polymers by solution intercalation where the nanoparticles are mixed with polymer in a common solvent [11], in-situ polymerization where the nanoparticles are mixed with monomer and then polymerized [12], and melt intercalation where the nanoparticles and polymer is mixed at temperatures well above the glass transition of the polymer [13, 14, 15]. Of these methods, melt intercalation is particularly attractive because it is compatible with current industrial processing equipment such as extruders and injection molders. In addition, the technique is environmentally and safety conscious due to the lack of organic solvent. All of the nanocomposites prepared in this work were prepared with melt intercalation.

1.2 Multicomponent polymer materials

In an effort to obtain polymeric materials with the desired properties for various applications, research and development over the past three decades has turned to polymer blending. Polymer blending uses existing polymers to create a material with a new property profile without the time and expense often needed to develop new monomers to synthesize a polymer with the same desired properties. For example, blending rigid polymer with a rubbery minor phase improves the impact resistance of the new material while maintaining stiffness within 25% of the neat rigid polymer [16, 17, 18, 19]. Blends can also be prepared with rigid polymers and crystalline polymers with increases in impact resistance while maintaining stiffness [20, 21].

Another way to obtain desired properties for a polymeric material is copolymerization. Copolymers contain structural units of two (or more) different monomers that are covalently bonded; how the monomer units are bonded together defines the type of copolymer. There are random copolymers (in which the monomer units are distributed randomly throughout the chain), graft copolymers (in which long segments of one polymer are grafted onto the other polymer at various points throughout the chain), and block copolymers (in which a long segment, or block, of polymer is bonded to the other polymer block at one point in the chain). Copolymers are similar to polymer blending in that existing products (monomers and polymers) are used to create a material with a new property profile. For example, ABS (acrylonitrile butadiene styrene), a random copolymer of poly(styrene-co-acrylonitrile) grafted onto polybutadiene, is tough and impact resistant while also being relatively strong and stiff [22].

Often both techniques can be combined to acquire a suitable material. Polymers are generally immiscible with each other due to the low entropy of mixing. When immiscible polymers are blended together, they phase separate to minimize the surface energy. These phase separated materials exhibit poor mechanical properties due to the weak interfacial adhesion between the two phases. Block or graft copolymers are often blended with the two immiscible polymers to improve the interfacial adhesion [18, 20, 21, 23, 24]. The copolymer segments are chosen such that one segment interacts favorably with one of the polymers, and the other segment interacts favorably with the other polymer.

1.3 Multicomponent polymer clay nanocomposites

Regardless of which polymers are combined and how they are combined, polymers tend to benefit from inorganic fillers like nanoclay. Similar to homopolymer nanocomposites, nanoclay can improve the mechanical and thermal properties of polymer blends and copolymers [25, 26, 27, 28, 29, 30, 31]. Nanoclay can also act as a compatibilizer in polymer blends [25, 26, 27, 28, 29]. In this work, both polymer blends and copolymers are studied with nanoclay.

1.3.1 Dielectric spectroscopy

In chapter two, clay nanocomposites based on styrene-butadiene-rubber (SBR) random copolymer are studied. Both components in the copolymer, styrene and butadiene, interact favorably with the nanoclay but to varying degrees. Polymer segments interacting with the nanoparticles relax more slowly than polymer segments in the bulk; this slower relaxation is detected using dielectric spectroscopy making it possible to use dielectric spectroscopy to quantitatively measure the degree of interaction between polymer and clay. By varying the composition of the copolymer and affinity of clay nanoparticles to each copolymer component, the degree of interaction between clay nanoparticles and each polymer component in the copolymer is determined. Dielectric spectroscopy analysis was also extended to diblock SBR copolymer nanocomposites, crosslinked SBR nanocomposites and SBR composites with carbon black.

1.3.2 Intercalation kinetics

In chapter three, static intercalation kinetics of SBR random copolymer and clay was studied using x-ray diffraction. The polymer components in SBR interact differently with clay, and the interactions of both components collectively determine how quickly the whole copolymer intercalates the clay. The intercalation kinetics of nanocomposites with varying SBR compositions were compared. The intercalation kinetics were also compared to the dielectric spectroscopy results from Chapter 2. There is a definite correlation between strong copolymer interaction (as measured by dielectric spectroscopy) and fast intercalation kinetics. Intercalation kinetic studies were extended to block copolymers and to sheared samples.

1.3.3 Blend compatibilization

Chapters four and five study the role of clay as a compatibilizer in different polymer blends. Chapter four covers blends of polyvinylidene fluoride (PVDF) and polyamide-6 (N6). The thermodynamic (i.e. interactions between the polymers and clay) and kinetic (i.e. melt viscosity of the polymers) factors that determine polymer blend morphology and thus polymer blend mechanical properties are discussed. In the blend nanocomposite with the best mechanical properties, the domain phase is amorphous with uniform, small domain sizes, and the clay nanoparticles are dispersed throughout the matrix and at the polymer-polymer interface. The knowledge from this work was applied to studies of polystyrene blends in chapter five. A similar result was found with polystyrene blends in that the toughest blends have the smallest, most uniform domain size.

BIBLIOGRAPHY

[1] Kojima, Y.; Usuki, A.; Kawasumi, M.; Okada, A.; Fukushima, Y.; Karauchi, T.; Kamigaito, O. *J. Mater. Res.* **1993**, *6*, 1185–1189.

[2] Fornes, T.; Paul, D. *Polymer* **2003**, *44*, 4993–5013.

[3] Yoon, P.; Fornes, T.; Paul, D. *Polymer* **2002**, *43*, 6727–6741.

[4] Lee, H.; Fasulo, P.; Rodgers, W.; Paul, D. *Polymer* **2006**, *47*, 3528–3539.

[5] Choi, W.; Kim, H.; Yoon, K.; Kwon, O.; Hwang, C. *J. Appl. Poly. Sci.* **2006**, *100*, 4875–4879.

[6] Yano, K.; Usuki, A.; Okada, A. *J. Polym. Sci. Part A: Polym. Chem.* **1997**, *35*, 2289–2294.

[7] Kim, S.; Kim, S. *J. Appl. Polym. Sci.* **2007**, *103*, 1262–1271.

[8] Gilman, J.; Jackson, C.; Morgan, A.; Harris, R.; Manias, E.; Giannelis, E.; Wuthenow, M.; Hilton, D.; Phillips, S. *Chem. Mater.* **2000**, *12*, 1866–1873.

[9] Gilman, J. *Appl. Clay. Sci* **1999**, *15*, 31–49.

[10] Zanetti, M.; Camino, G.; Thomann, R.; Malhaupt, R. *Polymer* **2001**, *42*, 4501–4507.

[11] Greenland, D. *J. Colloid Sci.* **1963**, *18*, 647–664.

[12] Usuki, A.; Kojima, Y.; Kawasumi, M.; Okada, A.; Fukushima, Y.; Kurauchi, T.; Kamigaito, O. *J. Mater. Res.* **1993**, *8*, 1179–1184.

[13] Vaia, R.; Ishii, H.; Giannelis, E. *Chem. Mat.* **1993**, *5*, 1694–1696.

[14] Vaia, R.; Giannelis, E. *Macromolecules* **1997**, *30*, 7990–7999.

[15] Vaia, R.; Giannelis, E. *Macromolecules* **1997**, *30*, 8000–8009.

[16] Wu, S. *Polymer* **1985**, *29*, 1855–1863.

[17] Joseph, S.; Thomas, S. *Eur. Polym. J.* **2003**, *39*, 115–125.

[18] Sardelis, K.; Michels, J.; Allen, G. *Polymer* **1987**, *28*, 244–250.

[19] Song, J.; Kim, J.; Suh, K. *J. Appl. Poly. Sci* **1999**, *71*, 1607–1614.

[20] Jannasch, P.; Wesslen, B. *J. Appl. Poly. Sci* **1998**, *70*, 1887–1891.

[21] Yoon, K.; Lee, H.; Park, O. *J. Appl. Polym. Sci.* **1998**, *70*, 389–395.

[22] Kim, H.; Keskkula, H.; Paul, D. *Polymer* **1991**, *32*, 1447–1455.

[23] Ansari, M.; Haghtalab, A.; Semsarzadeh, M. *Rheol. Acta.* **2006**, *45*, 983–993.

[24] Macosko, C.; Guegan, P.; Khandpur, A.; Nakayama, A.; Marechal, P.; Inoue, T. *Macromolecules* **1996**, *29*, 5590–5598.

[25] Si, M.; Araki, T.; Ade, H.; Kilcoyne, A.; Fisher, R.; Sokolov, J.; Rafailovich, M. *Macromolecules* **2006**, *39*, 4793–4801.

[26] Ray, S.; Pouliot, S.; Bousmina, M.; Utracki, L. *Polymer* **2004**, *45*, 8403–8413.

[27] Ryu, J.; Kim, H.; Lee, J. *Polym. Eng. Sci.* **2004**, *44*, 1198–1204.

[28] Chow, W.; Ishak, Z.; Ishiaku, U.; Karger-Kocsis, J.; Apostolov, A. *J. Appl. Poly. Sci.* **2004**, *91*, 175–189.

[29] Vo, L.; Giannelis, E. *Macromolecules* **2007**, *40*, 8271–8276.

[30] Laus, M.; Francescangeli, O.; Sandrolini, F. *J. Mater. Res.* **1997**, *12*, 3134–3139.

[31] Xu, H.; Li, Y.; Yu, D. *J. Appl. Polym. Sci.* **2005**, *98*, 146–152.

CHAPTER 2

DIELECTRIC STUDIES OF POLY(STYRENE-*CO*-BUTADIENE)/CLAY NANOCOMPOSITES

2.1 Introduction

Elastomers are used extensively industry and are often further enhanced by adding fillers such as carbon black. However, since carbon black reinforcement is inefficient and makes the material black (which is undesirable in certain applications), there have been efforts to replace carbon black with other fillers such as precipitated silica[1], inorganic[2] and organic[3] whisker fibers, carbon nanotubes[4], and layered silicate clays[5, 6, 7]. In this study, we focus on organically modified montmorillinite clay nanoparticles. Clay at a concentration of 10phr in natural rubber has been demonstrated by Okada et al. as having comparable tensile properties to 40phr of carbon black[7]. Clay rubber composites can also have better gas barrier properties[5] and vulcanization kinetics [6, 8] than pure rubber.

The rubber used in this study is poly(styrene-*co*-butadiene) also known as SBR (styrene-butadiene-rubber). When dispersing nanoparticles in a multicomponent polymer system such as SBR, it is important to know how each polymer component interacts with the nanoparticles. In polymer blend nanocomposites (which consist of nanoparticles and two non-covalently bonded polymer components), if the clay interacts favorably with only one polymer, then the nanoparticles resides only in that polymer phase[9]. However, with copolymer nanocomposites, if the clay interacts favorably with only one polymer, the nanoparticles can still be dispersed throughout the matrix[10]. In either case,

the time scale of dispersion (clay intercalation kinetics) maybe different from the separate homopolymers with clay. Interactions of each polymer component with clay affect nanocomposite processing and properties, so it is crucial that polymer-nanoparticle interactions for each polymer component be quantified within a copolymer and not just with homopolymers alone.

As crucial as SBR-filler interactions are to material properties, it is difficult to measure these interactions directly. Many researchers have inferred the strength of rubber-filler interactions by the amount of reinforcement in the rubber [11, 12, 13]. There have been other indirect analyzes of SBR-filler interaction such as measuring the amount of polymer adsorption from solvent onto substrate of filler [14], the crosslink density of composite, and the amount of swelling in solvent of composite [12]. More direct measurements of SBR-filler interaction have included using NMR spectroscopy to probe SBR motion close to carbon black particles [15]. In this study, SBR motion near clay nanoparticles is measured using dielectric relaxation spectroscopy.

Dielectric spectroscopy measures dipolar relaxation of polymers and is useful in studying polymer dynamics. Dielectric spectroscopy offers a wide range of frequencies and temperatures such that polymer dynamics can be measured over many different time/length scales. In this measurement, we focus on the segmental motion of the polymer chains. Several reviews and articles have summarized dielectric spectroscopy as applied to amorphous polymer systems [16, 17, 18]. As such, only short description and pertinent equations will be included here.

The complex dielectric function or permittivity of a system is defined as $\varepsilon^*(\omega) = \varepsilon'(\omega) + i\varepsilon''(\omega)$ where ε' is the real part of the function, ε'' is the imag-

inary (or loss) part, ω is angular frequency, and i = $\sqrt{-1}$. A relaxation is observed as a peak in a plot of the loss part, ε", as a function of frequency, $f = 2\pi\omega$. This peak is characterized by the Havrikliak-Negami (HN) function, a modified Lorentzian function. The fitting parameters for the HN function are β and γ, two shape parameters describing the width and symmetry of the peak and τ, the characteristic relaxation time related to the frequency at the maximum of the loss peak.

The temperature dependence of the relaxations is dependent on what motion is responsible for the relaxation. In this work, we focus on the α-segmental relaxation. α-segmental relaxation processes are responsible for dynamic glass transition and can thus be quantified by the glass transition temperature. To characterize the temperature dependence of α-segmental polymer relaxation, characteristic relaxation times, τ, are plotted for a series of different temperatures and fitted to the Vogel-Fulcher-Tammann (VFT) equation:

$$f = \frac{1}{\tau} \quad \propto \quad \exp\left(-\frac{\text{constant}}{T - T_\circ}\right) \tag{2.1}$$

where $T_\circ$ is the Vogel temperature (or the ideal glass transition temperature) and is found to be 30-70K below T_g. By convention, to calculate the glass transition temperature, T_g, from dielectric spectra, Equation 2.1 is extrapolated to the temperature at which τ = 100s [17, 18, 19].

When clay nanoparticles are added to SBR, in addition to the bulk segmental mode, there is a second, slower α relaxation mode present in the clay nanocomposites that is not present in pure SBR of any stoichiometry. We attribute this slower relaxation mode to the interfacially adsorbed chains of SBR on the surface of the clay nanoparticles. The strong interaction between the clay and polymer forces the chains near the clay to relax more slowly, with a new effective

interfacial glass transition temperature, T_{gi}, that is as much as 150°C higher than the bulk glass transition temperature, T_{gb}. Slower dynamics, as have been observed in similar studies, have been attributed to an interacting layer at the polymer-nanoparticle interface[20, 21, 22, 23]. This layer has been calculated from experimental results to be between 2-9nm[20, 21].

In this chapter, we use dielectric spectroscopy to measure interfacial glass transition temperatures as a means to quantify the interactions between polymers and nanoparticles. By varying copolymer composition and adding nanoparticles with different affinities for the two polymer components, we are able to measure interaction strength of each polymer component with clay nanoparticles. We then extend the analysis to crosslinked SBR nanocomposites and SBR nanocomposites with carbon black.

2.2 Experimental Part

For the studies involving copolymers of different compositions, the styrene-butadiene rubber (SBR) random copolymer blocks were provided by Lanxess or obtained from various sources as listed in Table 5.1. Also included in Table 5.1 are the characteristics of the one SBR block copolymer that was studied for comparison. All copolymers were processed similarly. The polymers were ground to 1mm particles, mixed with the appropriate amount of clay in a speed mixer, pressed into 20mm diameter, 1mm thick pellets at room temperature with a load of 150MPa, and annealed in a vacuum oven above the T_g (130°C for SBR composites and 160°C for PS composites).

For the studies involving crosslinking and carbon black, another SBR was

used. This SBR was provided by Michelin and contains 23% by weight styrene content. To differentiate this SBR from the one from Scientific Polymer Products, it will be referred to as mSBR23. Pellets of mSBR23 and clay are prepared and treated by the same process described in the previous paragraph. Michelin also provided composites prepared with their mixers. For analysis, pellets are cut from these samples. All cured samples were provided by Michelin. Curing agents include 2 parts zinc oxide, 2 parts SAD stearic acid, 1.5 parts sulfur, and 1.5 parts CBS, a sulfenamide based accelerator. Uncured samples from Michelin were heat treated to simulate the treatment of cured samples as well annealed samples at Cornell. Characteristics of this polymer and its mixes are listed in Table 2.2.

Modified montmorillonite clays (Cloisite 93A and Cloisite 20A) were obtained from Southern Clay Products and used as received. For dielectric studies, the clay amount was less than 5% by weight (to minimize signal from clay conductivity), and the pellet was annealed until complete intercalation was observed via x-ray diffraction. Clay diffraction spectra were collected on a Scintag Inc. $\theta - \theta$ diffractometer with a CuKα source ($\lambda = 1.54$Å) and a germanium detector, scanning at 3° min^{-1}.

Bulk glass transition temperatures calculated from dielectric spectroscopy were confirmed with a TA instruments Q1000 DSC scanning 10°C/min. Polymer relaxation was measured using dielectric spectroscopy with a Novocontrol N40 broadband spectrometer. Pellets of the annealed composite were placed between parallel gold plated electrodes 20mm (top) and 30mm (bottom) in diameter. Measurements swept through a frequency range of 1Hz to 10^6 Hz at isothermal conditions that varied from -100°C to 140°C.

Table 2.1: Characteristics of styrene and butadiene polymers and copolymers of varying compositions

sample	reference	M_w $\left(\frac{\text{kg}}{\text{mol}}\right)$	Source	T_{gb} (°C)
polybutadiene	PB	175	Lanxess	-96
5% styrene copolymer	SBR5	380	Sp[2]	-75
23% styrene copolymer	SBR23	547	Sp[2]	-63
45% styrene copolymer	SBR45	350	Sp[2]	-79
96% styrene copolymer	SBR96	167	Sigma-Aldrich	102
polystyrene	PS	192	Sigma-Aldrich	107
30% styrene block copolymer	SB30	54	Sigma-Aldrich	-95, 58
23% styrene copolymer	mSBR23	130	Michelin	-48

Dielectric relaxation modes are fit to the combination of power law and log normal functions totaling five parameters.

$$\varepsilon''(f) = \frac{f^a}{b} + e \exp -\left(\frac{\log f - \log c}{\log d}\right)^2 \tag{2.2}$$

a and b are two parameters belonging to the power law function, and they give the power law exponent (a) and the prefactor (b). The power law describes the conductivity of the composite stemming from the clay. c, d, and e are three parameters of the log normal function giving the mean, standard deviation, and scaling factor, respectively. The log normal component of the fit function can be extrapolated to the Havrikliak-Negami (HN) function. For the purposes of our analysis, only the peak frequency (mean) is used, so this simplified fit function is all that is necessary. The peak frequencies (f_{p}) are then converted to peak relaxation times (τ), and $-\ln(\tau)$ is plotted as a function of $1000/T(K)$. These points are fit to a VFT equation (Equation 2.1), and T_{g} is simply calculated from the fit.

Table 2.2: Characteristics of mixes of SBR with curing agents and additives

sample	20A clay	carbon black	curing agents?	cured?	heated?
mSBR23-20A	5 parts	0	n	n	n
mSBR23-20A-heated	5 parts	0	n	n	y
mSBR23-20A-Cornell	5 wt %	0	n	n	y
mSBR23-heated	0	0	n	n	y
mSBR23-curatives	0	0	y	n	n
mSBR23-cured	0	0	y	y	y
mSBR23-20A-curatives	5 parts	0	y	n	n
mSBR23-20A-cured	5 parts	0	y	y	y
mSBR23-CB	0	5 parts	y	y	y
mSBR23-20A-CB	5 parts	5 parts	y	y	y

2.3 Results and Discussion

2.3.1 SBR of varying composition with clay

The clay nanoparticles used in this work were modified via cation exchange with quaternary ammonium cations to render the clay surface more organophilic. The differences in the functional groups of the cations offer varying affinities to the polymer components in the copolymer. Cloisite 20A (herein referred to as 20A) is modified with dimethyl dehydrogenated di-tallow alkyl ammonium and intercalates both polystyrene and polybutadiene (Figure 4.1a). As both polymer components have favorable interactions with 20A clay, all of the studied SBRs with varying stoichiometry also intercalate 20A (Table 2.3). Cloisite 93A (herein referred to as 93A), modified with methyl dehydrogenated di-tallow alkyl ammonium is less polar than 20A and intercalates polybutadiene homopolymer but not polystyrene (Figure 4.1b). Since only one polymer component (butadiene) interacts favorably with 93A clay, the miscibility (intercalation) of SBR and 93A clay depends on the amount of butadiene in the

Table 2.3: Clay-SBR polymer miscibility (as determined by intercalation)

clay	PB	SBR5	SBR23	SBR45	SBR96	PS
20A	miscible	miscible	miscible	miscible	miscible	miscible
93A	miscible	miscible	miscible	miscible	not miscible	not miscible

copolymer. For the SBRs studied, SBR with 45% by weight styrene or less does intercalate 93A clay, but SBR with 96% by weight styrene does not intercalate (Table 2.3).

In these SBR polymer systems, dielectric spectroscopy measures the segmental dipole relaxation of polybutadiene (polystyrene has a weak dipole moment so its relaxation mode is eclipsed by that of polybutadiene). However, even though only one polymer component is probed, we can indirectly infer the interactions of the other polymer by studying SBRs of varying polymer compositions. For example, if butadiene is the component that is interacting more strongly with the nanoparticles, then the butadiene component relaxes more slowly and T_{gi} will increase with increasing butadiene concentration. Similarly, if the styrene component interacts more strongly with the nanoparticles, the styrene relaxes more slowly and T_{gi} will increase with increasing styrene concentration. Styrene interaction is being indirectly measured through butadiene relaxation dynamics; if styrene is being pinned due to strong interactions, butadiene will also "feel" the effects and its relaxation dynamics will slow down accordingly. In addition to varying polymer composition, by using two clays with different miscibilities, the interactions between each polymer component and the nanoclay can be studied.

As mentioned earlier, SBR clay systems display two segmental relaxation modes in dielectric spectroscopy. One of the modes is the bulk mode corresponding to α-segmental relaxation of the bulk polymers. Figure 2.2a shows the

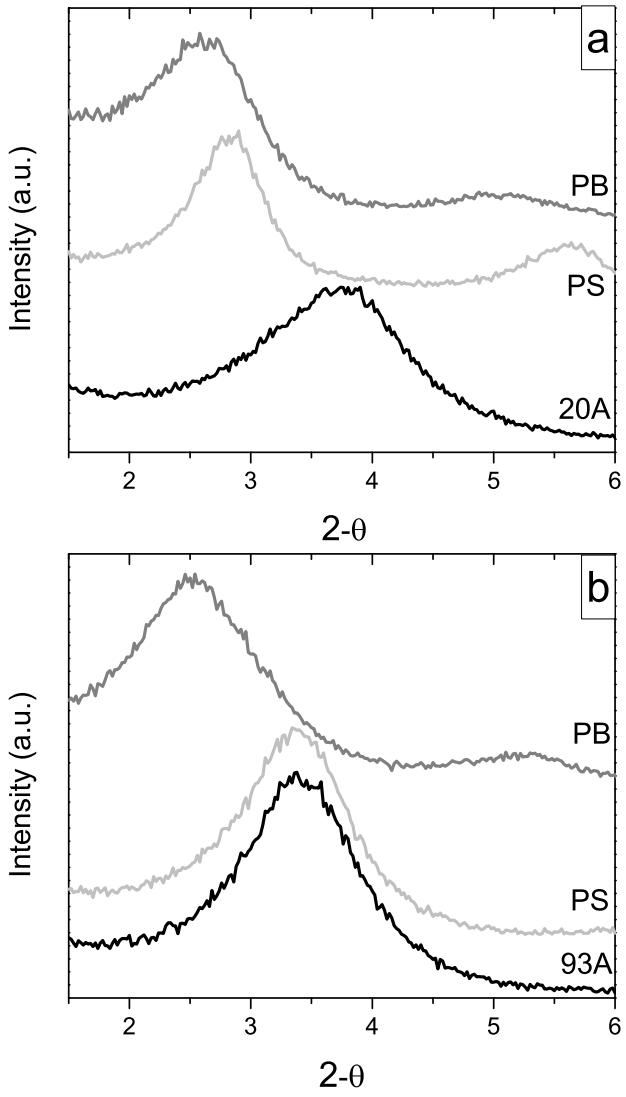

Figure 2.1: XRD plots of a) 20A clay and its composites polystyrene and polybutadiene and b) 93A clay and its composites with polystyrene and polybutadiene. 20A is intercalated by both polystyrene and polybutadiene homopolymers, while 93A is intercalated by only polybutadiene.

typical relaxation peaks of SBR at various temperatures. A T_{gb} is extrapolated from these peaks, and the result is similar to that measured with DSC (Table 5.1). When clay nanoparticles are added to SBR, the bulk segmental mode of SBR remains unchanged indicating that the bulk relaxation motion is not disturbed. The other, slower mode, present only in samples with clay, is an interfacial mode corresponding to the relaxation of polymer near the clay nanoparticles. Figure 2.2b shows the relaxation peaks for SBR23-20A clay nanocomposite at temperatures ranging from 30 – 90°C. (These temperatures are higher than those shown in Figure 2.2a of the bulk segmental mode, and in the same frequency window, higher temperatures correspond to slower modes).

The relaxation times, τ, for each interfacial relaxation peak are plotted as a function of temperature in Figure 2.3 for 20A nanocomposites. (Equation 2.1 has been fit to the data, and the fits are included with the data in Figure 2.3). 20A is miscible with both homopolymers and the tested copolymers. However, as seen in Figure 2.3, each nanocomposite has a different temperature dependence indicating different interactions with the 20A clay. For example, in Figure 2.3, the fit for PB-20A falls at lower temperatures than SBR5-20A extrapolating to a lower T_{gi} for PB-20A than for SBR5-20A. The extrapolated T_{gi} for those nanocomposites as well as the other copolymer nanocomposites are plotted in Figure 2.4 as a function of styrene content. The trend for 20A composites follows that T_{gi} increases as styrene concentration increases. The lowest T_{gi} among this group of polymers corresponds to homopolymer polybutadiene and 20A with T_{gi} = 19°C. Even with the lowest T_{gi}, the glass transition of the interfacial mode is still 115°C above the bulk glass transition of the bulk mode for polybutadiene with 20A. This indicates favorable interactions between 20A clay and butadiene components which is evidenced by PB/20A intercalation.

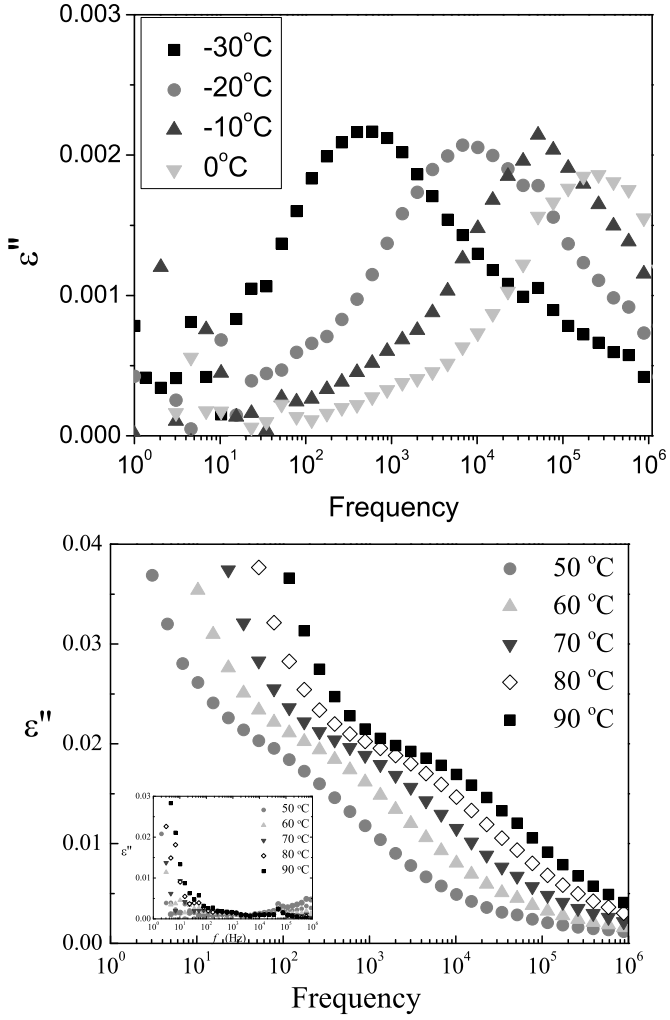

Figure 2.2: a) Dielectric loss, ε", of SBR23 at temperatures ranging from −30°C to 0°C. b) Dielectric loss, ε", of SBR23 with 20A clay at temperatures ranging from 30 to 90°C. Higher temperature relaxations in the same frequency range indicate a slower polymer relaxation. This relaxation is only present in SBR with clay; the inset shows ε" for SBR23 without clay in the same temperature range. This slower relaxation is attributed to interfacially adsorbed chains on the surface of the clay nanoparticles.

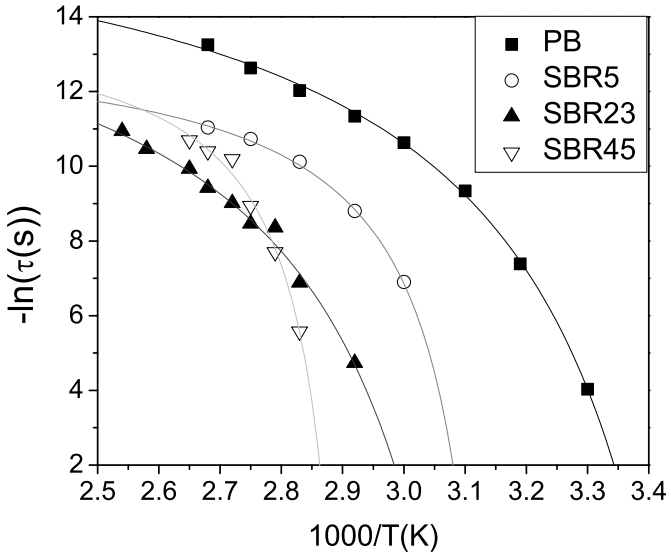

Figure 2.3: Interfacial relaxation times as a function of temperature for 20A clay composites with SBR polymers of varying styrene content. Lines are VFT (Equation 2.1) fits to the data. Interfacial glass transition temperatures (T_{gi}) are extrapolated from the fits at $-\ln(\tau = 100\text{s}) = -4.6$. Polybutadiene has the lowest T_{gi} and SBR45 has the highest.

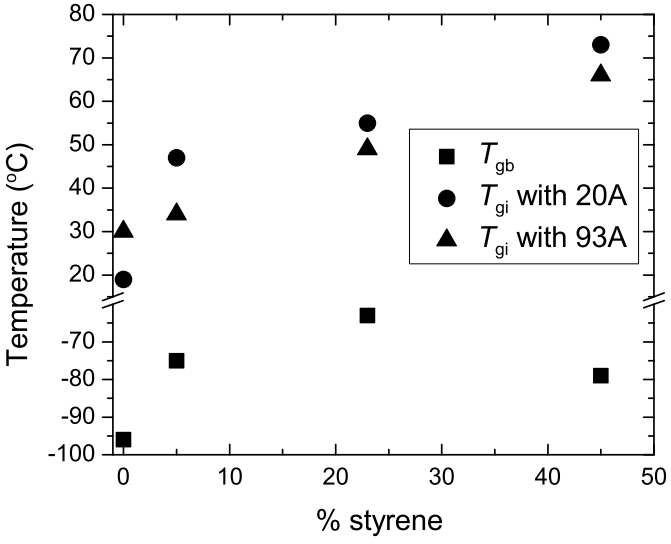

Figure 2.4: Interfacial and bulk glass transition temperatures for SBRs of varying compositions with 20A and 93A. T_{gi} increases as styrene content increases for both 20A and 93A clay, while T_{gb}varies with styrene content within a smaller temperature range. T_{gi} is larger for 20A compared to 93A at every SBR composition.

Continuing through the composition spectrum, SBR5 copolymer with just 5% styrene has a $T_{gi} = 47^{\circ}$ which is 28° higher than T_{gi} of PB and 20A. This indicates that styrene component interacts strongly with the clay, more so than the butadiene component. Strong styrene-silicate interaction is attributed to polar interactions as previously studied though theoretical modeling[24], and systematic experiments into melt intercalation[25] and intercalation kinetics[26]. Alkene (butadiene) groups also offer polar interactions but not as strongly as aromatic (styrene) groups. Strong silicate-styrene interactions are further evidenced with SBRs with higher concentrations of styrene. SBR23 with 20A and SBR45 with 20A containing 23% and 45% styrene, respectively, have T_{gi} of $53^{\circ}$and 73°, respectively. This increase in T_{gi} with increasing styrene content does not appear to be related only to corresponding higher bulk glass transition temperatures. Also shown in Figure 2.4 are T_{gb} for each polymer; while T_{gi} increase, T_{gb} are within a small range. So while T_{gb} for different SBRs plateaus, T_{gi} increase as the styrene content increases.

The other clay, 93A, intercalates homopolymer polybutadiene but not polystyrene. 93A clay is modified by a tertiary ammonium surfactant whereas 20A is modified by a quaternary ammonium. The hydrogen in 93A allows the surfactant to hydrogen bond to the silicate surface. This bonding is quite favorable reducing the surfactant mobility[27]. With an immobilized surfactant, there are fewer sites for a more polar polymer such as polystyrene to interact with the surface. Clay intercalation is dependent on three pairwise interacting parameters: ϵ_{sa}, the interaction between the clay surface and the aliphatic chains of the surfactant, ϵ_{sp}, the interaction between the surface and the polymer chains, and ϵ_{ap}, the interaction between the surfactant and the polymer. Favorable surface-polymer and, to some extent, surfactant-polymer interactions

are necessary for intercalation compared to surface-surfactant interactions [24]. In the case of 93A, the hydrogen bonding and immobilized surfactant reduce the area of surface-polymer interaction minimizing the contribution of ϵ_{sp}. One way to overcome the reduced contribution of ϵ_{sp} is to increase the contribution of ϵ_{ap}. For example, polystyrene intercalates 10A clay. 10A is modified with a di-methyl benzyl hydrogenated tallow, which is a quaternary ammonium. 10A is modified with a benzyl group which interacts favorably with polystyrene potentially assisting intercalation. However, the benzyl group also interacts favorably with the surface reducing the number of contact sites, similar to the hydrogen bonding with 93A. In the case of 10A clay though, the added surfactant-polymer interaction overcomes the reduced contribution of ϵ_{sp}.

To gauge the extent of the reduced contribution of ϵ_{sp} for 93A clay, polymers of varying polarity were shear mixed with 93A. Three six-carbon ringed polymers were tested: polystyrene, polyvinylcyclohexane (PVCH), and polybromostyrene (PS3Br). Polybutadiene was also included. In order of polarity, PVCH $\ll$ PB $<$ PS $<$ PS3Br. The only polymer miscible with 93A is PB. PS3Br does have strong surface-polymer interactions, but the reduction in interacting surface area combined with the unfavorable surfactant-polymer interactions prevent PS3Br from intercalating 93A. To a lesser extent, this is also the case for PS. PVCH, on the other hand, is essentially non-polar and does not interact with the surface. It does interact with the surfactant but these interactions are only van der Waals forces and are not enough to drive intercalation alone. PB offers a compromise in polarity. The double bonds provide some favorable interactions with the oxygens on the silicate surface. PB also interacts favorably with alkanes[28] which are present in the surfactant as hydrogenated tallow groups. Similar to PS-10A nanocomposite, butadiene interactions with both the surface

and surfactant lead to intercalation of 93A by polybutadiene. Ultimately, the type of polymer that can intercalate 93A is limited by the reduction in area of surface-polymer interaction. However, the following paragraphs describe how copolymers can overcome this limitation.

In the copolymer series, SBR5, SBR23, and SBR45 are all miscible with 93A, but SBR96 is not. This is not surprising as the SBR96 contains 96% styrene component whereas the other SBRs contain less than 50% styrene. If butadiene is the only component that is interacting with the nanoclay and driving intercalation, then it is expected that T_{gi} will remain the same (or decrease) with increasing styrene concentration. However, this is not the case as seen in Figure 2.4. As styrene concentration increases, T_{gi} for 93A composites also increases. T_{gi} for 93A composites with PB, SBR, SBR23, and SBR45 are 30°, 34°, 49°, and 66°, respectively. Increasing T_{gi} with styrene concentration indicates that 93A clay is interacting with a component (styrene) that it is incompatible with in the homopolymer form.

Upon closer examination, 93A has only one hydrogen with which to hydrogen bond leaving some sites with a less favorable methyl (from surfactant)-oxygen (from silicate surface) interaction (similar to 20A clay). If styrene could access these sites, the replacement of methyl-oxygen interaction with aromatic-oxygen interaction is more favorable. For homopolymer polystyrene, accessing the sites is not energetically favored. However for styrene-butadiene random copolymer, there are butadiene segments which interact with the aliphatic chains (hydrogenated tallow groups) in the gallery. Once the polymer is inside the gallery, styrene segments are in proximity to the accessible sites on the silicate surface with which they can interact.

Block copolymers of styrene and butadiene offer a way to evaluate the role of interdispersed styrene segments in random copolymers by providing a point of contrast. In block copolymers, the styrene segment is not dispersed throughout the chain but is instead concentrated at one end of the chain bonded to butadiene only at one point. SB30, a block copolymer with 30% styrene, is miscible with both 20A and 93A. XRD studies of these nanocomposites show that the clays intercalate to approximately the same d-spacing and FWHM (Figure 2.5). Dielectric spectroscopy of these two nanocomposites reveal two very different results though. SB30-93A interfacial relaxation is much slower than that of SB30-20A (Figure 2.6). T_{gi} of SB30-93A is 25°compared to 60° for SB30-20A. Comparing the interfacial glass transition temperatures of the block copolymer nanocomposites with T_{gi} of the random copolymer nanocomposites, there is a similarity between SB30-93A and PB30-93A and between SB30-20A and SBR23-20A. The similarity between SB30-93A and PB-93A implies that only the butadiene segment is interacting with the clay and thus butadiene is the only segment that has intercalated. This possibility would not necessarily show up in XRD as butadiene comprises 70% of the chain and given the molecular weight and approximated monomer size and polymer structure, the majority of the clay surface would still be covered even if only the butadiene block were to intercalate. If this is the case, it suggests that there is a limit to the length of styrene segment that can be intercalated with butadiene. 93A clay does not offer enough accessible interacting sites per unit area to accommodate longer styrene segments such as styrene-butadiene block copolymer or homopolymer styrene.

In the case of the other clay, both blocks of SB30 are compatible with 20A and both are likely to be intercalated. The addition to the styrene block in the gallery greatly reduces polymer mobility as styrene interacts strongly with the surface.

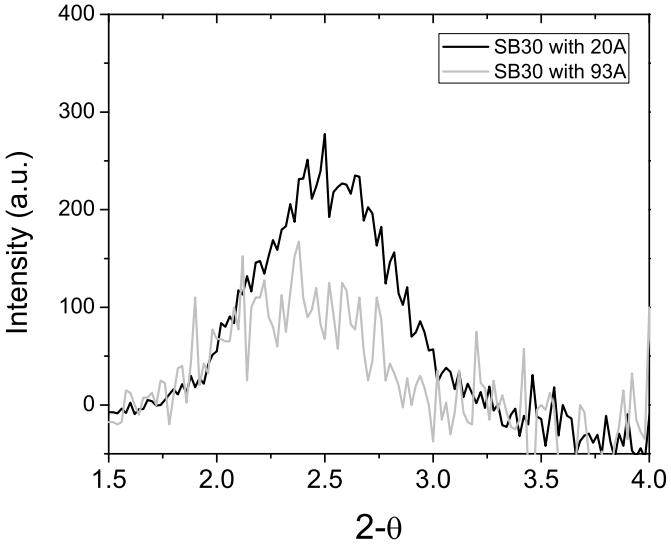

Figure 2.5: XRD plots of SB30 with 20A and 93A clays. SB30 intercalates both 20A and 93A clays to approximately the same d-spacing.

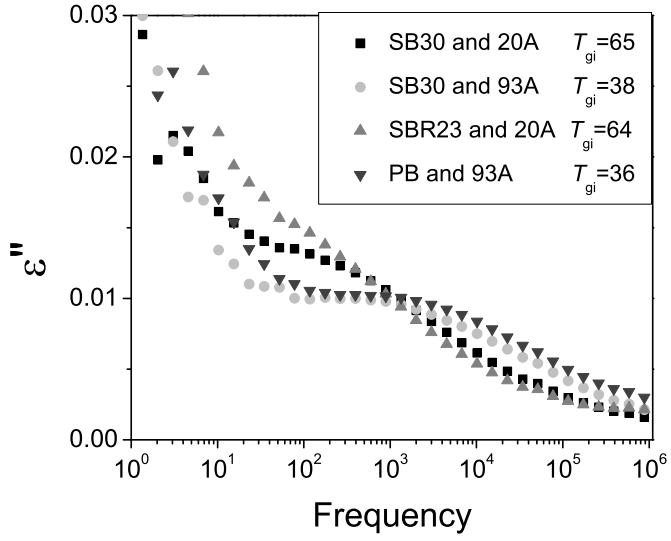

Figure 2.6: Interfacial relaxation mode at $T = 80°$ of SB30 block copolymer with 20A and 93A as well as SBR23 with 20A and PB with 93A for reference. SB30-20A relaxes more slowly than SB30-93A. SB30-20A relaxation more closely resembles that SBR23-20A, whereas SB30-93A more closely resembles PB-93A.

Unlike 93A, 20A offers more accessible sites with each styrene can interact. T_{gi} of SB30-20A is nearly identical to that of SBR23-20A, a random copolymer with a comparable styrene concentration. This observation suggests that when both segments are compatible with the clay nanoparticles, the copolymer structure is not crucial to polymer-clay interactions. Applying a similar comparison between 93A and 20A clay for SBR random copolymers (Figure 2.4) reveals that for each SBR in the series, SBR-20A T_{gi} is higher than T_{gi} for SBR-93A like in the case of SB30. However for random copolymers, the difference is not as dramatic as the styrene segments are dispersed through the chain. SBR-20A nanocomposites have higher T_{gi} than SBR-93A nanocomposites because 20A provides more replacement sites than 93A. With more replacement sites, there are more polymer-clay interactions resulting in slower polymer dynamics.

Dielectric spectroscopy essentially probes the number of contacts between the polymer and silicate surface. Thermodynamically, greater numbers of favorable contacts leads to an increasingly negative internal energy of the nanocomposite system. Following the model set forth by Vaia[24], the change in internal energy upon polymer intercalation is represented by

$$\Delta E = A^{f}_{sp}\epsilon_{sp} + A^{f}_{ap}\epsilon_{ap} + (A^{f}_{sa} - A^{i}_{sa})\epsilon_{sa} \tag{2.3}$$

where s, p, and a correspond to the components silicate surface, polymer, and aliphatic chains, respectively. A^{i}_{jk} and A^{f}_{jk} are the total area of contact between the components for the initial unintercalated system and final intercalated system, respectively, and ϵ_{jk} is the pairwise interaction energy for the components with negative values of ϵ_{jk} indicating favorable interactions. Both ϵ_{jk} and A_{jk} play a role in intercalation. For example, in this work, the clay surface of 93A and polystyrene interact favorably, but the hydrogen bonding surfactant reduces the interacting surface area therefore reducing the internal energy of the

system preventing intercalation. In addition to internal energy, entropy also contributes to the free energy. However, in the formation of a intercalated hybrid, the entropy loss from polymer intercalation is balanced by entropy gain of the surfactant molecules from layer separation[25]. Thus favorable interactions play a dominant role in the free energy of nanocomposite formation, and dielectric spectroscopy serves as a tool for quantifying these favorable interactions.

2.3.2 Crosslinked SBR with clay

In real world applications, SBR is usually crosslinked as the cured polymer provides more desirable mechanical properties. Crosslinked polymers have slower dynamics which are also possible to study with dielectric spectroscopy. In this section, the effect of curatives and crosslinking on bulk and interfacial polymer dynamics is studied.

The difference between crosslinked SBR nanocomposites and uncrosslinked nanocomposites is more than just the crosslinks themselves. To crosslink SBR, curing agents are mixed with SBR, and after mixing, the samples are then heated to activate the curing. The heat treatment in addition to the additives can affect polymer dynamics as much as the crosslinking. To rule out, or at least assess, these effects, various control samples were also studied.

The first controls are mSBR23 samples without clay; one sample has not been heat treated, mSBR23, and one sample has, mSBR23-heated. Representative dielectric relaxation curves and T_{gb} for these two samples are shown in Figure 2.7a. After heat treatment, mSBR23 has a slower bulk mode ($T_{gb} = -39°C$) compared to mSBR23 with no heat treatment ($T_{gb} = -53°C$). For rubber un-

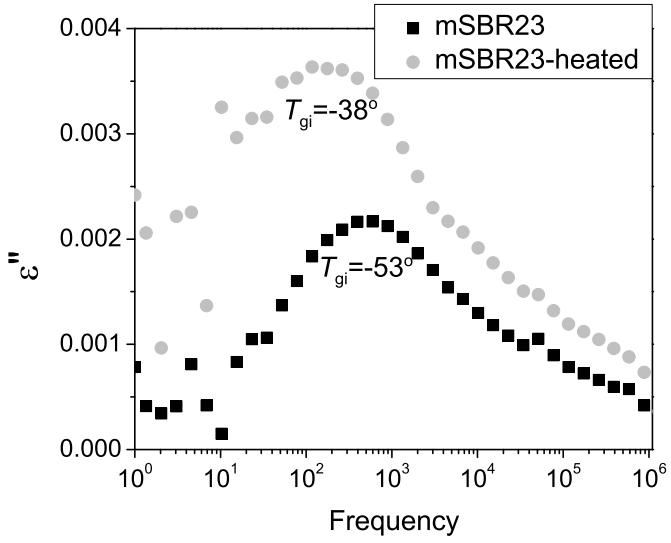

Figure 2.7: Dielectric loss relaxation for mSBR23 and mSBR23-heated at −30°C. Neat mSBR23-heated has a slower relaxation than mSBR23 with no heat treatment.

dergoing extended heat treatment (~ 24 hours), slower bulk polymer dynamics most likely indicates crosslinking as crosslinks are known to slow down polymer motion [29]. However, this slower motion is still not as slow as the interfacial polymer motion studied in the previous sections (T_{gi} > 30°), and measurements at temperatures typical of interfacial polymer motion reveals no mode (Figure 2.7b).

A similar comparison was carried out on mSBR23 samples with clay. The three samples in this control batch are: mSBR23-20A with no heat treatments or additives, mSBR23-20A-heated, that has been heat treated, and mSBR23-20A-Cornell prepared by pressing and heat treatment at Cornell (instead of by mixer at Michelin). Both the bulk and interfacial relaxation modes were compared. T_{gb} and T_{gi} for the three samples as well as representative relaxation peaks are shown in Figure 2.8. Bulk glass transition temperatures were all within 5° of the DSC measurement (−48°) indicating that neither the mixing process nor heating affects bulk polymer relaxation in uncured nanocomposite samples. This

result differs from the results of mSBR23 (without clay). While T_{gb} of mSBR23 is also within 5° of the DSC measurement, T_{gb} of mSBR23-heated is not (Figure 2.7). These results suggest that while heat treatment initiates crosslinking in neat mSBR23, the addition of clay hinders crosslinking even with heat treatment. Studies of vulcanization kinetics completed elsewhere are not consistent with regards to whether clay nanoparticles enhance [6, 8] or impede [30, 31] crosslinking. However, all of those studies include curatives such as sulfur which these control samples do not contain. In this case, crosslinking is likely related to the thermal stability of the SBR. Clay nanoparticles have been shown to enhance the thermal stability of nanocomposites [32, 33], and in rubber nanocomposite, it seems as though thermal stability (lack of decomposition) prevents rubber crosslinking.

There is also a difference in interfacial glass transition temperatures between heat-treated and not heat-treated composites. T_{gi} for mSBR23-20A is 17° whereas T_{gi} for the heat treated samples are 30° for mSBR23-20A-heated and 39° for mSBR23-20A-Cornell. Heat treatment appears to provide better contact between nanoparticles and polymer resulting in slower polymer dynamics compared to a mix with no heat treatment. The small difference between the two heat treated samples is attributed to the difference in mixing processes. mSBR23-20A-heated was mixed with a rotary mixer and annealed in an oven whereas mSBR23-20A-Cornell was pressed and annealed in the oven. The difference suggests that pressing provides better contact between nanoparticles and polymer than mixing.

The next comparison is between the previous samples which contain no curatives with a sample that does contain curing agents. mSBR23-curatives is a

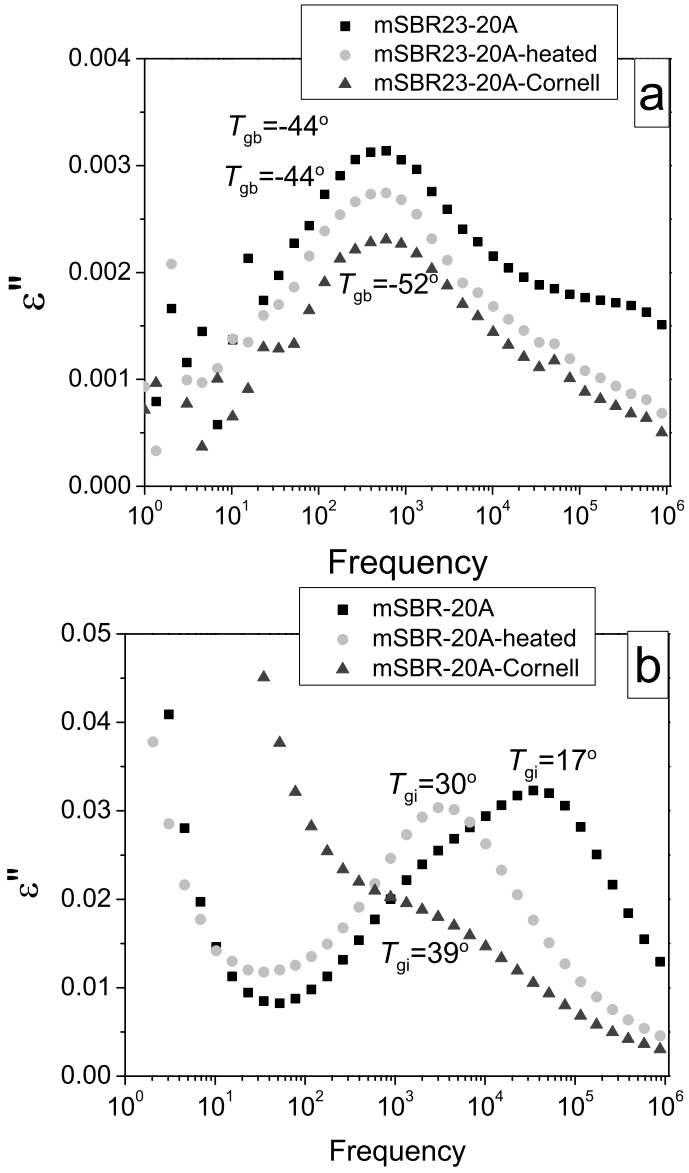

Figure 2.8: a) Bulk relaxation modes at $T = -30°C$ and b) interfacial relaxation modes at $T = 80°C$ for mixes of mSBR23 and 20A clay. Heat treatment and different mixing processes do not affect bulk relaxation. Heat treatment does affect the interfacial relaxation; samples that have been heat treated have slower relaxation dynamics.

sample with curatives but has not been cured. T_{gb} is −46° and similar to the bulk glass transition of the samples with no curatives indicating that the curing agents themselves do not affect the bulk polymer dynamics. mSBR23-cured is chemically the same mix as mSBR23-curatives, but it has been crosslinked. As mentioned earlier, bulk polymer dynamics are expected to slow down as polymer motion is restricted by crosslinking. Figure 2.9a shows the relaxation peaks of both mSBR23-curatives and mSBR23-cured, and the relaxation peak for mSBR23-cured is at a lower frequency than mSBR23-curatives confirming expectations. T_{gb} for the cured sample is −37°, higher than the non-cured sample. Another thing to note is that T_{gb} for mSBR23-cured is close to T_{gb} for mSBR23-heated (−39°) confirming that the slower bulk polymer dynamics of mSBR23-heated is due to crosslinking by heat.

A similar comparison is made with composites containing both curatives and 20A clay: mSBR23-20A-curatives has curatives but has not been cured and mSBR23-20A-cured has been cured. Comparing the bulk mode of both cured and uncured samples, T_{gb} for mSBR23-20A-curatives and is within two degrees of T_{gb} for mSBR23-curatives (no 20A), and T_{gb} for mSBR23-20A-cured is within two degrees of mSBR23-cured indicating that clay does not affect bulk polymer dynamics in both cured and uncured SBR. Comparing the interfacial mode of cured and uncured samples (Figure 2.9b), T_{gi} for mSBR23-20A-curatives and mSBR23-20A-cured is 37° and 36°, respectively, indicating that curing does not affect interfacial polymer dynamics as it does for bulk polymer dynamics. SBR bulk polymer motion is much faster than interfacial polymer motion. When SBR is crosslinked, the faster bulk motion is constrained by the links (from T_{gi} = −44° for uncrosslinked to T_{gi} = −35° for crosslinked). However, the interfacial polymer dynamics are so much slower (T_{gi} = 37°) than crosslinked SBR motion

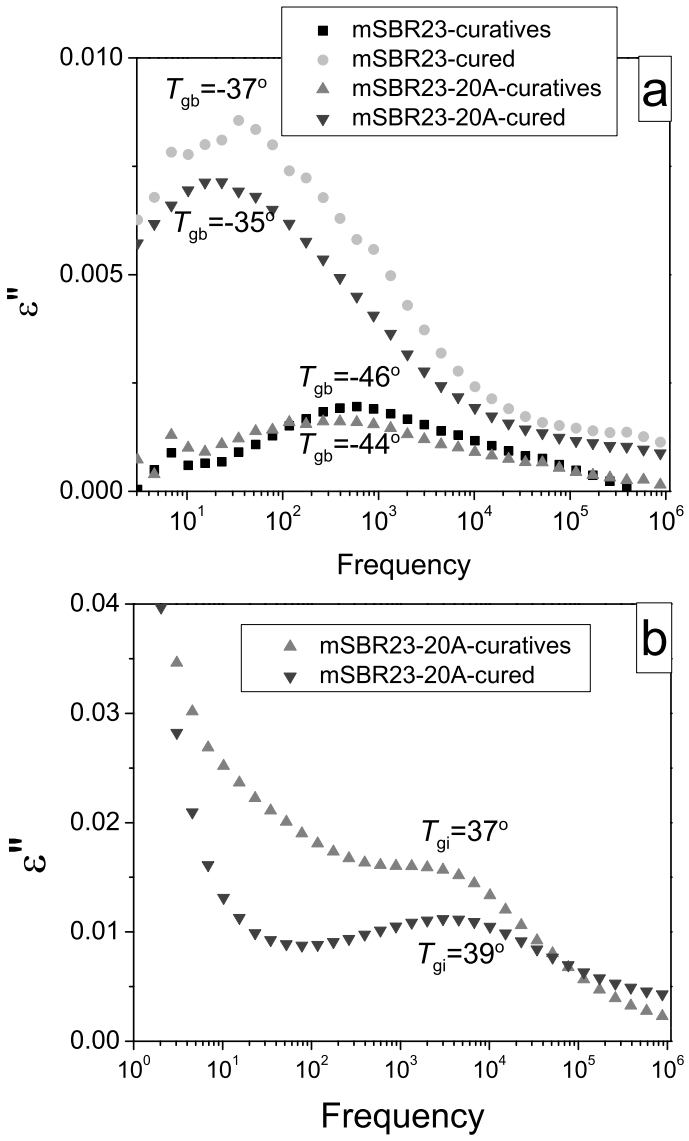

Figure 2.9: a) Bulk relaxation modes at $T = -30$°C and b) interfacial relaxation modes at $T = 80$°C of samples with curatives (but have not been cured) and samples that have been cured. Crosslinking slows bulk polymer dynamics but has no effect on interfacial polymer dynamics. Neither the bulk or interfacial relaxations are affected by the curatives themselves.

that the interfacial polymer dynamics are not affected by crosslinking.

2.3.3 SBR with clay and carbon black

A major application of SBR is in tires, and tires are generally formulated with a large (> 30%) amount of carbon black. In this section, dielectric spectroscopy is applied to SBR samples with carbon black (CB) in an attempt to quantify this important SBR-CB interaction. As clay is likely to be used in addition to carbon black, at least in the interim, it is also useful to assess how carbon black affects polymer-clay interaction.

Carbon black is conductive, and the signal from the conductivity can mask the signal from polymer relaxation. To curtail this effect, the concentration of carbon black is kept low (at 5 parts) instead of at the concentrations normally used in industry. Figure 2.10 shows a region of dielectric signal for a sample of mSBR23-CB-cured at temperatures where clay-polymer interfacial mode is normally seen. There is a small shoulder in this region, and the position of this shoulder appears to change with temperature. However, the signal is just too weak and the conductivity is too high to conclusively state whether there is a carbon black-SBR signal. While studies have shown that there is interaction between carbon black and SBR [11, 14, 15], the interaction is weak. The large amounts of carbon black typically used in industry is to overcome this weak interaction and achieve the desired properties.

Even though carbon black interactions cannot be measured directly, its effect on clay can still be measured. Figure 2.11 compares the interfacial relaxation mode of a sample with carbon black and clay (mSBR23-20A-CB-cured)

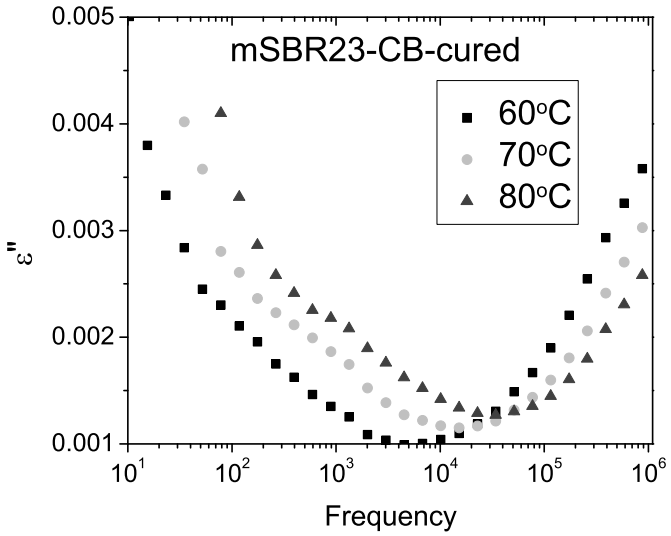

Figure 2.10: Dielectric relaxation of mSBR23 and carbon black from 60 to 80°C. There is no distinct interfacial mode for mSBR23-carbon black interactions.

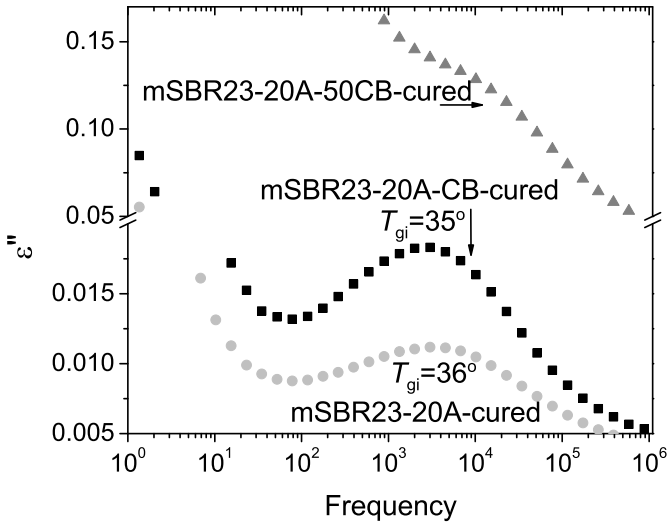

Figure 2.11: Interfacial relaxation at 80°C of mSBR23 with 5phr carbon black, SBR with clay and 5phr carbon black, and SBR with clay and 50phr carbon black. Carbon black does not affect the clay-SBR interfacial relaxation.

to that of a sample with only clay. The peaks appear to be in the same location, and calculated T_{gi} are also almost identical at 36° for the sample with clay and 35° for the sample with carbon black and clay. A sample of higher carbon black concentration (50phr) and clay was also tested (mSBR23-20A-50CB). While the high conductivity of this amount of carbon black completely masks any potential carbon black-SBR interfacial relaxation peaks, clay-SBR peaks are still distinguishable (Figure 2.11). Unfortunately T_{gi} could not be calculated for these peaks because of the high conductivity, but the peaks of mSBR23 with no carbon black and mSBR23 with 50phr of carbon black appear to be at similar frequencies. This result suggests that carbon black, even in large amounts, does not affect clay-polymer interaction.

2.4 Summary

Dielectric relaxation spectroscopy was used to measure SBR and SBR nanocomposite polymer dynamics. Both the bulk and interfacial polymer relaxations were measured and quantified by the glass transition temperatures associated with the motion. The interfacial polymer relaxed much more slowly than the bulk polymer due to its interactions with the nanoparticle surface. SBRs of different compositions were tested with clay (20A) that is intercalated by both polystyrene and polybutadiene homopolymers. In this case, even though both components of SBR interact favorably with 20A, SBR with higher styrene concentration had slower polymer dynamics indicating that the styrene component of SBR interacts more strongly with the clay than the butadiene component.

The same experiment was repeated with a clay (93A) that is intercalated by

polybutadiene homopolymer but not polystyrene. Even in this case, styrene still interacts favorably with the clay. 93A does not offer as many accessible sites with styrene to interact with so homopolymer polystyrene does not intercalate it, but if butadiene segments enter the gallery, styrene segments can access the sites and interact with the clay. This only works with small styrene segments such as the ones found in random SBR. Polymer dynamics of SBR block copolymer and 93A resemble that of homopolymer polybutadiene and 93A. Head-to-head comparisons between 20A and 93A reveal that polymer dynamics of SBR-93A are slower than SBR-20A because 93A does not have as many accessible sites to interact with as 20A.

The polymer dynamics of crosslinked SBR were also studied. Crosslinking slows down bulk polymer dynamics but not interfacial polymer dynamics. Curatives themselves (not the crosslinks) do not affect either the bulk or interfacial relaxation. Clay nanoparticles prevent thermal decomposition and crosslinking of neat SBR exposed to heat but do not affect vulcanization. The addition of carbon black does not affect the bulk or clay-interfacial modes. Carbon black interaction with SBR is very weak compared to clay and could not be measured with dielectric spectroscopy.

BIBLIOGRAPHY

[1] O'Haver, J.; Harwell, J.; Evans, L.; Waddell, W. *J. Appl. Polym. Sci.* **1996**, *59*, 1427–1435.

[2] Zhou, Z.; Liu, S.; Gu, L. *J. Appl. Polym. Sci.* **2001**, *80*, 1520–1525.

[3] Nair, K.; Dufresne, A. *Biomacromolecules* **2003**, *4*, 666–674.

[4] Bokobza, L. *Polymer* **2007**, *48*, 4907–4920.

[5] Usuki, A.; Tukigase, A.; Kato, M. *Polymer* **2002**, *43*, 2185–2189.

[6] Arroyo, M.; Lopez-Manchado, M.; Herrero, B. *Polymer* **2003**, *44*, 2447–2453.

[7] Okada, A.; Usuki, A.; Kurauchi, T.; Kamigaito, O. ACS Symposium Series: Hybrid Organic-Inorganic Composites, 1995.

[8] Choi, D.; Kader, M.; Cho, B.; Huh, Y.; Nah, C. *J. Appl. Poly. Sci.* **2005**, *98*, 1688–1696.

[9] Vo, L.; Giannelis, E. *Macromolecules* **2007**, *40*, 8271–8276.

[10] Chen, H.; Schmidt, D.; Pitsikalis, M.; Hadjichristidis, N.; Zhang, Y.; Wiesner, U.; Giannelis, E. *J. Polym. Sci. Part B: Polym. Phys.* **2003**, *41*, 3264–3271.

[11] Kraus, G. Reinforcement of Elastomers, New York, NY, 1965; pp 125–151.

[12] Bala, P.; Samantaray, B.; Srivastava, S.; Nando, G. *J. Appl. Polym. Sci.* **2004**, *92*, 3583–3592.

[13] Edwards, D. *J. Mat. Sci.* **1990**, *25*, 4175–4185.

[14] Kraus, G.; Dugone, J. *Ind. Eng. Chem.* **1955**, *47*, 1809–1816.

[15] Dutta, N.; Choudhury, N.; Haidar, B.; Vidal, A.; Donnet, J.; Delmotte, L.; Chezeau, J. *Polymer* **1994**, *35*, 4293–4299.

[16] Schonhals, A. Dielectric spectroscopy of polymeric materials, Washington, D.C., 1997; pp 81–106.

[17] Bello, A.; Laredo, E.; Grimau, M. *Phys. Rev. B* **1999**, *60*, 12764–12774.

[18] Schuller, J.; Mel'nichenko, Y.; Richert, R.; Fischer, E. *Phys. Rev. Lett.* **1994**, *73*, 2224–2227.

[19] Roland, C.; Casalini, R. *J. Chem. Phys.* **2003**, *119*, 1838–1842.

[20] Arrighi, V.; McEwen, I.; Qian, H.; Serrano Prieto, M. *Polymer* **2003**, *44*, 6259–6266.

[21] Tsagaropoulos, G.; Eisenberg, A. *Macromolecules* **1995**, *28*, 6067–6077.

[22] Xu, W.; Raychowdhury, S.; Jiang, D.; Retsos, H.; Giannelis, E. *Small* **2008**, *4*, 662–669.

[23] Carretero-Gonzalez, J.; Retsos, H.; Giannelis, E.; Ezquerra, T.; Hernandez, M.; Lopez-Manchado, M. *Soft Matter* **2009**, *5*, 3481–3486.

[24] Vaia, R.; Giannelis, E. *Macromolecules* **1997**, *30*, 7990–7999.

[25] Vaia, R.; Giannelis, E. *Macromolecules* **1997**, *30*, 8000–8009.

[26] Manias, E.; Chen, H.; Krishnamoorti, R.; Genzer, J.; Kramer, E.; Giannelis, E. *Macromolecules* **2000**, *33*, 7955–7966.

[27] Heinz, H.; Vaia, R.; Krishnamoorti, R. *Chem. Mater.* **2007**, *19*, 59–68.

[28] Tausendfreund, I.; Bandermann, F.; Siesler, H.; Kleimann, M. *Polymer* **2002**, *43*, 7085–7091.

[29] Kramarenko, V.; Ezquerra, T.; Sics, I.; Balta-Calleja, F.; Privalko, V. *J. Chem. Phys.* **2000**, *113*, 447–452.

[30] Zheng, H.; Zhang, Y.; Peng, Z.; Zhang, Y. *Polym. Test.* **2004**, *23*, 217–223.

[31] Kader, M.; Nah, C. *Polymer* **2004**, *45*, 2237–2247.

[32] Zanetti, M.; Camino, G.; Thomann, R.; Malhaupt, R. *Polymer* **2001**, *42*, 4501–4507.

[33] Gilman, J. *Appl. Clay. Sci* **1999**, *15*, 31–49.

CHAPTER 3

INTERCALATION KINETICS OF POLY(STYRENE-*CO*-BUTADIENE)/CLAY NANOCOMPOSITES

3.1 Introduction

Melt intercalation is a convenient technique for synthesizing polymer-clay nanocomposites. This is especially true in industry due to its compatibility with current processing techniques. Melt intercalation involves annealing polymer and clay nanoparticles above the melting or glass transition temperature of the polymer; the anneal can be done statically or with shear. Intercalation kinetics of melt intercalation, how quickly the polymer chains in the melt state penetrate clay nanoparticles, as a function of temperature, shear, and polymer molecular weight have been measured with a variety of polymers using different methods. Vaia et al. [1] studied polystyrene and organically modified clays with x-ray diffraction and transmission electron microscope. They found polymer mass transport to the primary particle controlled intercalation kinetics and observed that the temperature dependence of polymer diffusion into the gallery was similar to bulk polystyrene. Manias et al. [2] followed up on that work and found that polymer intercalation diffusivity scales as the inverse of molecular weight and is faster than neat polymer which has a different molecular weight dependence. The effect shear on intercalation has been studied with complex shear in an extruder [3], steady shear in a rheometer [4], and dynamic shear in a rheometer [5, 6]. These works has been extended elsewhere to polypropylene thermoplastic [7, 8], polar polybutylene terephthalate [5], and epoxy thermosets [9] using rheological measurements [5, 7, 8] in addition to x-ray diffraction.

In this work, clay intercalation kinetics for polystyrene-co-polybutadiene random copolymer (also known as styrene-butadiene-rubber or SBR) of varying compositions are monitored with x-ray diffraction. Copolymers have more than one polymer component to interact with the clay nanoparticles. Each polymer component has a different affinity for the clay and plays a role in whether the copolymer intercalates and how quickly it intercalates. In addition to different SBRs, clays with different miscibilities in polystyrene and polybutadiene homopolymers are also studied. By comparing effective polymer intercalation diffusivities (D_{eff}) among different polymer-clay combinations, the type of polymer-clay interactions that drive intercalation can be inferred. However, not only are diffusivities compared among each other, they are compared with the interfacial glass transition temperatures (T_{gi}) of the same polymer-clay combinations calculated in Chapter 2 from dielectric spectroscopy relaxation spectra. T_{gi} gives a quantitative measure of interaction strength between polymer and clay which can be linked to intercalation kinetics.

3.2 Experimental Part

The polymers used for kinetic studies are the same as those used for dielectric spectroscopy. The table listing their characteristics is listed again in Table 5.1 of this chapter for reference. The same clays, Cloisite 93A and Cloisite 20A obtained from Southern Clay Products, are used in this study. The steps for characterizing polymers by DSC and preparing polymer nanocomposite pellets are covered in Chapter 2. The difference for the pellets in kinetic studies is that the pellets contain 30% clay by weight as opposed to 5% (to increase the x-ray signal), and the pellets are not annealed prior to kinetic studies.

Intercalation kinetics were studied *ex-situ* as reported previously; SBR-clay pellets were annealed in a vacuum oven and removed periodically to collect diffraction spectra. Diffraction spectra were collected on a Scintag Inc. $\theta - \theta$ diffractometer with a CuKα source (λ = 1.54Å) and a germanium detector, scanning at 3°min^{-1}. The results are fit using the same equations and protocols outlined previously [1]. The kinetics are interpreted with an effective diffusion coefficient, D_{eff}, which is calculated from fitting the fraction of intercalated hybrid to the following equation,

$$\chi(t) \equiv \frac{I(t)}{I(\infty)} = 1 - \sum \frac{4}{a_m} \exp\left(-\frac{D_{\text{eff}}}{\overline{a}^2} a_m t\right)$$

where $\frac{I(t)}{I(\infty)}$ is the ratio of polymer intercalated at time t to polymer intercalated at equilibrium, $\overline{a}$ is the mean silicate size, and a_m are the roots of the zeroth order Bessel function. D_{eff} was calculated with a mean silicate size of 5μm.

Kinetic studies with shear were completed with Michelin SBR (see Table 5.1). mSBR and 30% clay were combined into pellets in an identical manner to forming pellets for static kinetic studies. The pellets were sheared in an Ares parallel plate rheometer at 10rad/s, 20% strain, and 150°C under flowing nitrogen. The amount of time shear was applied depended on the clay; shear time ranged from 30 minutes to 16 hours. The degree of intercalation at various points on the pellet was measured with the Nanostar small angle x-ray scattering (SAXS) equipment. Data was collected on a 2-dimensional detector for 1hour and averaged through all angles. Total shear displacements were calculated as the arc length at the radius where a measurement was taken.

3.3 Results and Discussion

3.3.1 Kinetic studies and the relation to interfacial interaction

SBR of varying composition with clays of different miscibilities

The clay nanoparticles used in this work were modified via cation exchange with quaternary ammonium cations to render the clay surface more organophilic. The differences in the functional groups of the cations offer varying affinities to the polymer components in the copolymer. Cloisite 20A (herein referred to as 20A) is modified with dimethyl dehydrogenated di-tallow alkyl ammonium and intercalates both polystyrene and polybutadiene homopolymers. Cloisite 93A (herein referred to as 93A), modified with methyl dehydrogenated di-tallow alkyl ammonium is less polar than 20A and intercalates polybutadiene homopolymer but not polystyrene. Since all of the SBRs studied contain 45% styrene or less, all SBRs are miscible with 93A. However, even though all SBRs intercalate 93A, the kinetics of intercalation may be different depending on copolymer composition due to different affinities of polybutadiene and polystyrene to 93A.

The percentage of intercalated 20A clay as a function time is shown in Figure 3.1 for the SBRs of varying composition as well as the two homopolymers. Effective diffusional rate constants, $\frac{D_{\text{eff}}}{\overline{a}^2}$, fit to each set of data are listed in Table 3.2. Assuming $\overline{a} = 5\mu$m, the effective diffusivities, D_{eff}, for each composite are also listed in Table 3.2. (The mean primary particle size, $\overline{a}$, was determined by TEM from previous studies [1] but was not verified for each composite in this study). As the styrene content increases, 20A intercalation kinetics acceler-

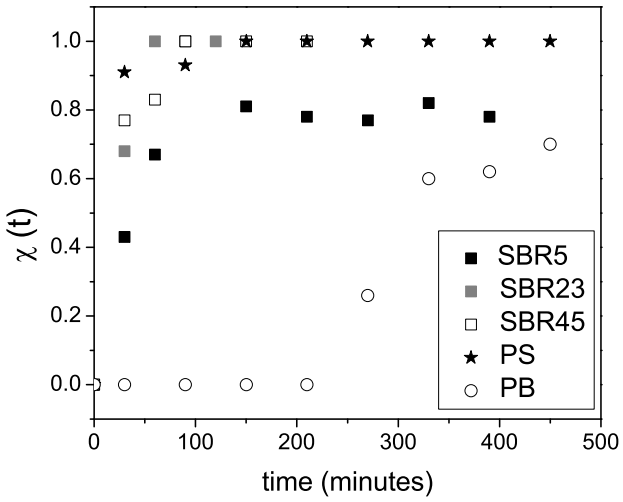

Figure 3.1: Intercalation kinetics of SBRs of varying composition with 20A. PB intercalates 20A more slowly than polymers with styrene. The effective diffusion coefficients vary as follows: PB < SBR5 < SBR23 ~ SBR45 < PS.

ates. Polybutadiene (no styrene present) exhibits a lag time of over 200 minutes before intercalation with the effective diffusivity constant of all the polymers intercalating 20A. SBR5 (with 5% styrene content) does not experience the same lag time before intercalation and its diffusivity is an order of magnitude larger than that of PB-20A. The effective diffusivity constants of SBR23 and SBR45 with 20A are comparable with each other and larger than SBR5. PS intercalates 20A slightly faster than SBR23 and SBR45. Polystyrene intercalation of 20A is faster than polystyrene self diffusion at 170°C ($D \sim 10^{-11} \frac{\text{cm}^2}{\text{s}}$) [1]. This result has been observed previously [2] and is attributed to the attractive interactions between polystyrene and the silicate surface. Higher diffusion rates are even observed in SBR nanocomposites where the styrene content is diluted with butadiene. Both SBR23 and SBR45 intercalate clay faster than if self diffusion of polystyrene controlled intercalation. Only when the styrene content of SBR is reduced to 5% is the diffusivity constant of SBR5-20A comparable to polystyrene diffusion in the bulk.

Polybutadiene, on the other hand, intercalates 20A more slowly than it would if self diffusion controlled intercalation ($D \sim 10^{-10}\frac{cm^2}{s}$ at $T = 100°C$) [10]. Polybutadiene has a considerably lower glass transition temperature than polystyrene, and at these processing temperatures is more mobile than polystyrene. Similar to how interactions between polystyrene and clay results in a larger effective diffusion coefficient compared to PS self diffusion [2], perhaps the interactions between polybutadiene and clay are to account for the slower kinetics. To bring more insight to the situation, dielectric spectroscopy measurements are compared to the kinetic measurements. As covered in Chapter 2, dielectric spectroscopy serves as a tool for quantifying interactions. These interactions contribute to the internal energy change upon nanocomposite formation and ultimately the change in free energy. The change in free energy dictates whether a nanocomposite is formed and how quickly it is formed. Valignat et al.[11] studied the kinetics of polymer wetting an inorganic substrate, and Manias et al.[2] extended that work to polymer-clay intercalation by writing an expression for the effective diffusivity constant as

$$D_{\text{eff}} \sim \frac{\Delta G_W}{\zeta} \tag{3.1}$$

where ΔG_W is the difference in the free energy between the polymer melt outside the silicate gallery and the polymer inside the gallery and ζ is the friction coefficient of polymer motion on the silicate surface.

As a review of the dielectric spectroscopy results, SBRs with more styrene content had higher T_{gi} indicating more favorable polymer-clay contacts. More favorable polymer chains-silicate surface contacts would translate to a more negative free energy and by equation 3.1, faster intercalation. Figure 3.2 plots both the effective diffusivity constants and interfacial glass transition temperatures as a function of styrene content. D_{eff} and T_{gi} follow the same trend in that

both increase as styrene content increases. T_{gi} for PB-20A and SBR5-20A are 19° and 47°C, respectively, for a difference of 28°. There is a corresponding large difference in D_{eff} for the same nanocomposites; D_{eff} for SBR5-20A is an order of magnitude larger than PB-20A. While polybutadiene does interact with 20A (as evidence by the interfacial mode relaxation), the interactions are not nearly as favorable as polystyrene and 20A. This could account for the large difference in intercalation kinetics between polybutadiene and the polymers with styrene content.

Applying the same comparison among the other copolymers does not reveal the same dramatic differences. While T_{gi} increases steadily for SBRs with higher styrene content, D_{eff} for the same nanocomposites increases little with styrene content. Following the same reasoning as above, SBR45 (with 45% styrene) provides more styrene-clay contact sites than SBR23 or SBR5 and should have faster kinetics. However, even though T_{gi} for SBR45-20A is higher than that for SBR23-20A, SBR45 does not intercalate 20A faster than SBR23. The diffusivity constants for these two polymers are comparable with one another at $1.0 * 10^{-10} \frac{cm^2}{s}$ and $1.1 * 10^{-10} \frac{cm^2}{s}$ for SBR23-20A and SBR45-20A, respectively. Homopolymer polystyrene intercalates 20A at a slightly higher, but similar, rate ($1.8 * 10^{-10} \frac{cm^2}{s}$) indicating that the intercalation kinetics have "plateaued" or slowed in their increase. Even though samples with higher styrene content contain additional favorable interactions to increase the kinetics, the larger number of aromatic-silicate interactions may also increase the friction coefficient, and diffusion kinetics are inversely proportional to friction (Equation 3.1). In this case, energetic gains by SBR45-20A intercalation balance the increase in friction, and the intercalation kinetics are comparable to SBR23-20A.

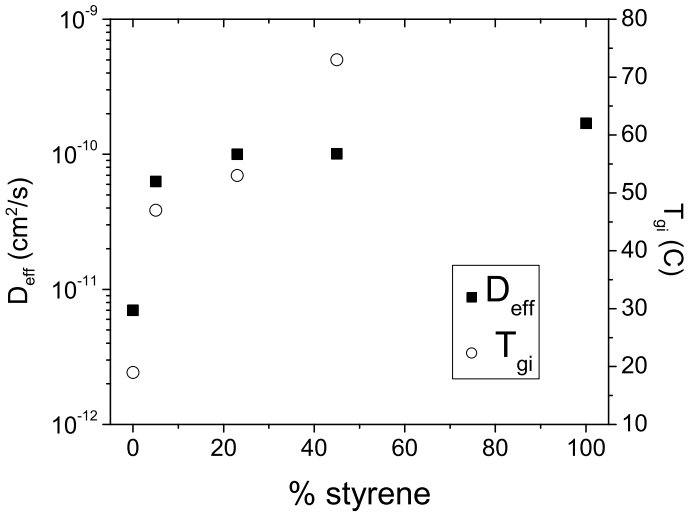

Figure 3.2: Effective diffusion coefficients (left axis) and interfacial glass transition temperatures (right axis) for SBR and 20A as a function of SBR styrene content. Both D_{eff} and T_{gi} increases as styrene concentration in the copolymer increases.

The other clay, 93A, is miscible with homopolymer polybutadiene but not polystyrene. The SBRs studied are miscible with 93A. Figure 3.3 shows the intercalation kinetics of the miscible polymers. Table 3.2 lists the effective diffusional rates and constants for these composites as well. Both PB and SBR5 experience a lag time before intercalating 93A; the diffusion coefficients for PB-93A and SBR5-93A are the same order of magnitude (10^{-12}). Recall that SBR5 did not experience a lag time to intercalation for 20A. Dielectric spectroscopy measurements give some insight as to a possible reason for the discrepancy between SBR5-93A and SBR5-20A. Direct comparison of T_{gi} of SBR5-20A and SBR5-93A shows T_{gi} of SBR5-93A is lower than SBR5-20A (34°C compared to 47°C). Lower T_{gi} indicates fewer contact sites for SBR5-93A. 93A clay contains a tertiary ammonium surfactant that hydrogen bonds with the clay surface. It is likely that hydrogen bonding reduces the number of contact sites for 93A compared to 20A clay. Reduced contact sites corresponds to a smaller free energy change upon intercalation and slower kinetics. Thus, 5% styrene content is not enough to speed

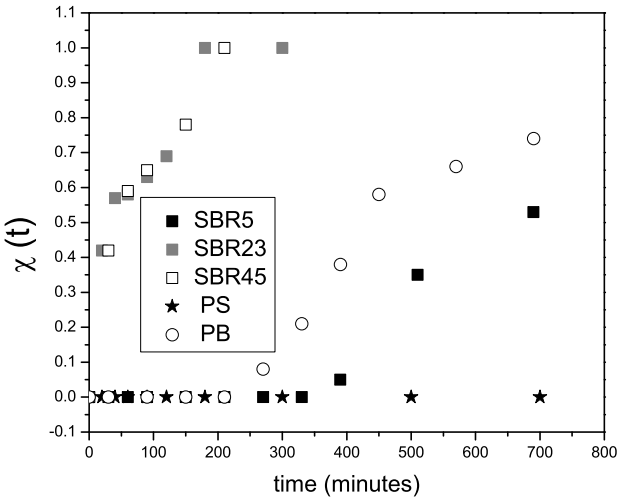

Figure 3.3: Intercalation kinetics of SBRs of varying composition with 93A

up intercalation kinetics of 93A due to the reduced number of contact sites for 93A.

Another comparison worth making is between PB and SBR5. Whereas the difference between T_{gi} for PB-20A and SBR5-20A is 28°, the difference between PB-93A and SBR5-93A is only 4°. This correlates very well with the large jump in D_{eff} between PB-20A and SBR5-20A but not between PB-93A and SBR5-93A (see Figure 3.4 for D_{eff} and T_{gi} versus styrene content for 93A nanocomposites). It should also be noted that SBR5-93A actually has a slightly longer lag time compared to PB-93A, but this is likely due to the higher molecular weight of SBR5 (380kg/mol) compared to PB (175kg/mol). In the case of 20A and SBR5, the addition of more favorable interactions counteract the larger molecular weight.

Continuing through the composition spectrum with 93A, SBR23 and SBR45 do not experience a lag time before intercalation. Similar to 20A, SBR23 and SBR45 have comparable diffusion coefficients. SBR-93A nanocomposite intercalation kinetics also seem to plateau with increasing styrene content similar to

Table 3.1: Characteristics of styrene and butadiene polymers and copolymers of varying compositions

sample	reference	M_w $\left(\frac{\text{kg}}{\text{mol}}\right)$	Source	T_{gb} (°C)
polybutadiene	PB	175	Lanxess	-96
5% styrene copolymer	SBR5	380	Sp^2	-75
23% styrene copolymer	SBR23	547	Sp^2	-63
45% styrene copolymer	SBR45	350	Sp^2	-79
polystyrene	PS	192	Sigma-Aldrich	107
30% styrene block copolymer	SB30	54	Sigma-Aldrich	-95, 58
23% styrene copolymer	mSBR23	130	Michelin	-48

Table 3.2: Effective diffusional rate constants $\left(\frac{^{D}\text{eff}}{\bar{a}^2}\right)$ and diffusivities (D_{eff}) for SBR polymers with different clays.

Polymer	20A		93A	
	$\frac{^{D}\text{eff}}{\bar{a}^2}\left(\text{s}^{-1}\right)$	$D_{\text{eff}}\left(\frac{\text{cm}^2}{\text{s}}\right)$	$\frac{^{D}\text{eff}}{\bar{a}^2}\left(\text{s}^{-1}\right)$	$D_{\text{eff}}\left(\frac{\text{cm}^2}{\text{s}}\right)$
PS	0.00067 ± 0.00015	$1.8 * 10^{-10}$	n/a	
SBR45	0.00043 ± 0.00007	$1.1 * 10^{-10}$	0.00021 ± 0.00004	$5.3 * 10^{-10}$
SBR23	0.00040 ± 0.00003	$1.0 * 10^{-10}$	0.00030 ± 0.00007	$7.5 * 10^{-11}$
SBR5	0.00025 ± 0.00004	$6.3 * 10^{-11}$	0.000014 ± 0.000002	$3.5 * 10^{-12}$
PB	0.000028 ± 0.000002	$7.0 * 10^{-12}$	0.000020 ± 0.000007	$5.0 * 10^{-12}$

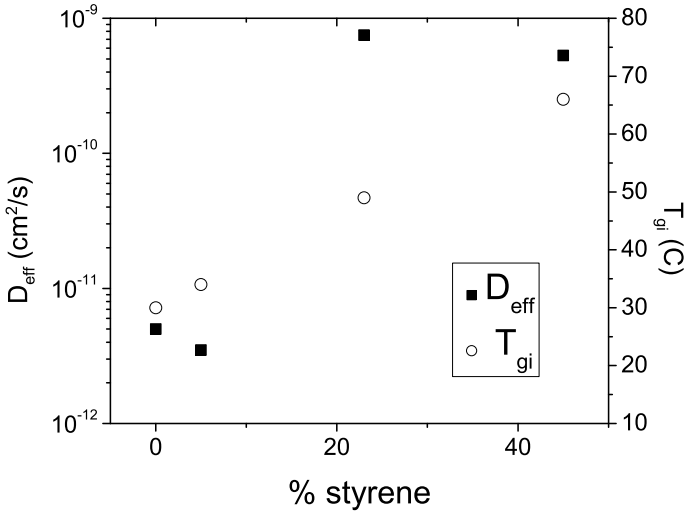

Figure 3.4: Effective diffusion coefficients (left axis) and interfacial glass transition temperatures (right axis) for SBR and 93A as a function of SBR styrene content

SBR-20A. Direct comparisons between 93A and 20A nanocomposites at these higher concentrations of styrene (23% and 45%) reveal even more similarities. The diffusion coefficients for these SBR23-20A and SBR23-93A are comparable, and by the property of transitivity, the diffusivities of SBR45-20A and SBR45-93A are also comparable. While at lower concentrations of styrene there were dramatic differences in D_{eff}, the influence of friction reduces the differences at higher concentrations.

SBR block copolymer with clays of different miscibilities

Diblock copolymers consist of two different polymer blocks covalently bonded at one point. The segments are generally very long (depending on the copolymer composition) and are localized at one end of the chain. This differs from random copolymers where polymer segments are much shorter and are dispersed throughout the chain. The difference in chain architecture between block and random copolymers can lead to vastly different behavior between the two. For example, while the addition of $\sim 20-30\%$ styrene into a random copolymer greatly increases the kinetics of intercalation of the random copolymer compared to polybutadiene (Figures 3.1 and 3.3), the addition of 30% styrene into a block copolymer does not change the kinetics of intercalation compared to PB (Figure 3.5). Figure 3.5 shows the intercalation kinetics of SB30, a styrene-butadiene diblock copolymer with 30% styrene, in both 20A and 93A clay. The intercalation kinetics of SB30 and 20A is nearly identical to SB30 and 93A with both nanocomposites experiencing a lag time before intercalation; the lag times to intercalation for SB30 nanocomposites are comparable to the lag times for PB-20A and PB-93A.

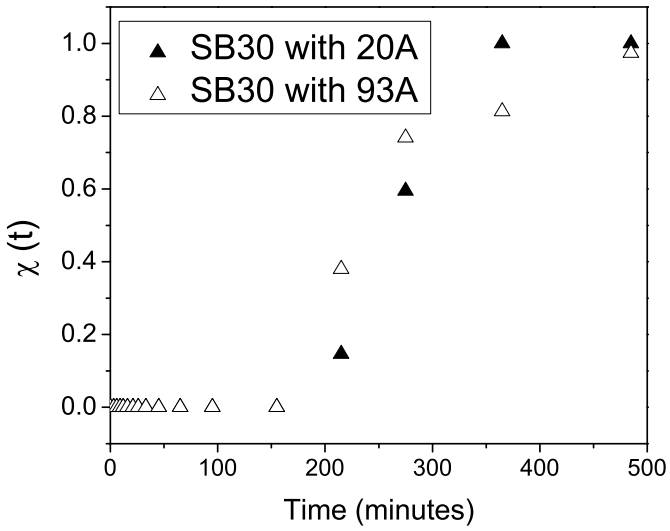

Figure 3.5: Intercalation kinetics of SB30 with 20A and 93A. SB30 intercalates both 20A and 93A at approximately the same rate. Both nanocomposites experience a lag time before intercalation similar to PB-20A and PB-93A.

Similar to how different polymer relaxations (T_{gi}) corresponded to different intercalation kinetics (D_{eff}) for random copolymers, dielectric spectroscopy can also be applied to the kinetic study of block copolymers. T_{gi} of SB30-93A is comparable to T_{gi} of PB-93A (25° compared to 30°). The kinetic behavior of SB30-93A and PB-93A is also similar to each other with comparable lag times. Recall that 93A does not intercalate polystyrene homopolymer. The styrene block of SB30A is long and resembles homopolymer polystyrene. In SBR random copolymer, the styrene segments are short and can be brought inside the gallery by the favorable interactions between the butadiene and the surfactant chains. However, because of the block architecture, the styrene segment of SB30 is too long for the butadiene segment to bring inside the gallery, and thus only the butadiene segment intercalates 93A. With only butadiene intercalating, both the intercalating kinetics and the dielectric relaxation of SB30-93A resembles that of PB-93A.

In the case of 20A clay, the dielectric relaxation behavior of SB30-20A does

not correspond with its kinetic behavior. The high interfacial glass transition temperature of SB30-20A (60°) indicates that SB30-20A should have fairly fast kinetics. However, in this case, the kinetics of SB30 is limited by its architecture. Homopolymer polystyrene intercalates 20A quickly (Figure 3.1), but the styrene segment of SB30 comprises only 30% of the chain. Given the composition and molecular weight of SB30, even if the entire styrene block were to intercalate, only ~ 25nm of clay would be intercalated which is less than 3% of the lateral dimension of the clay layers (~ 1μm). Such a small amount of intercalation is unlikely to be measured with x-ray diffraction, thus intercalation kinetics (as measured by XRD) is limited by how quickly the butadiene segment can be intercalated. Polybutadiene intercalates 20A slowly, and so does SB30. Because styrene interacts more favorably with clay, having styrene segments dispersed throughout the chain (random copolymer) results in faster intercalation kinetics than having them concentrated at one end.

3.3.2 Shear effects on intercalation kinetics

In industry, polymers are generally processed with shear using equipment such as extruders, mixers, and millers. In this section, the effect of shear on mSBR23 intercalation kinetics is studied. Shear is also applied to polymer-clay combinations known to not intercalate statically to observe whether or not shear can reduce the activation energy barrier to intercalation.

mSBR23 is miscible with both 20A and 93A. Intercalation kinetics of mSBR23 under static conditions are shown in Figure 3.6. mSBR23 intercalates 20A slowly but with no (measurable) lag time to begin intercalation. However, there is a

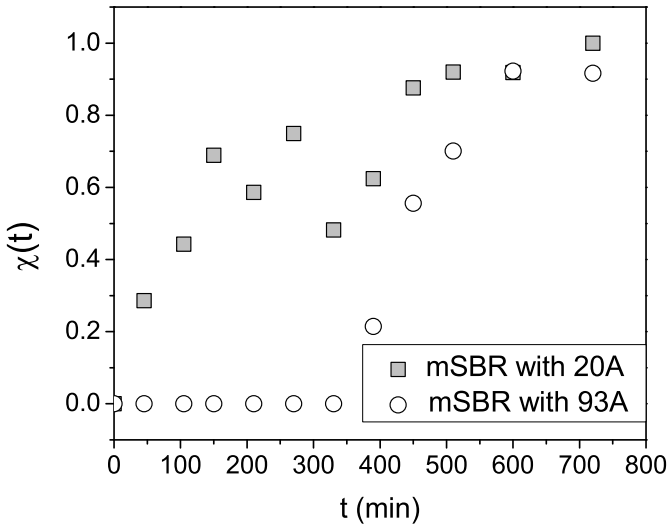

Figure 3.6: Static intercalation kinetics of mSBR23 with 20A and 93A. mSBR23 intercalates 20A slowly with no measurable lag time. mSBR23 does not begin to intercalate 93A until t = 300minutes.

lag time to intercalation of 93A. This plot serves as a reference with which is compare intercalation with shear.

To control other variables such as temperature and anneal time while shearing, different amounts of strain need to be applied all at once to the same sample. By centering a SBR-clay pellet between two circular plates of a rheometer, different amounts of strain are applied to different radii of the pellet. The middle of the pellet experiences little to no strain while the outer edge experiences the most strain.

mSBR23-20A was sheared for 30 minutes. As shown in Figure 3.6, at t = 30 minutes, mSBR23 has begun to intercalate 20A, but the intercalation is only $\sim$ 30% complete. If shear does not affect intercalation, then the intercalation process should be $\sim$ 30% complete at every point on the pellet. However, this is not the case. Figure 3.7 shows x-ray diffraction spectra for mSBR23 and 20A at different points along the pellet. The spectra are clearly different from each

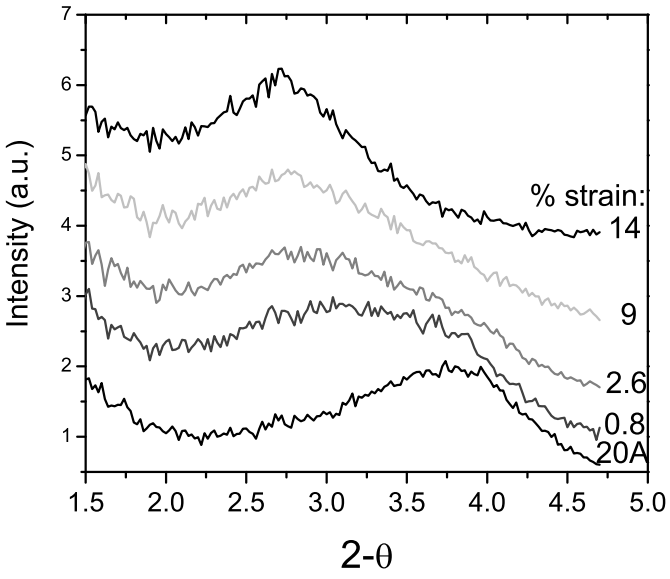

Figure 3.7: SAXS diffraction spectra for mSBR23 with 20A at different amounts of strain. Regions of more strain are further intercalated than regions with less strain.

other with the clay in regions of more strain being further intercalated than clay in regions of less strain. The fraction of intercalated clay calculated from these spectra is plotted in Figure 3.8 as a function of strain. The intercalation behavior is gradual as function of strain with slightly more strain resulting in a slightly more intercalated nanocomposite. This behavior is similar to the intercalation fraction as a function of time (see inset or Figure 3.6). At ~ 0% strain, the intercalation process is ~ 40% complete, similar to the static experiment at t = 30 minutes. At higher amounts of strain, the intercalation process is further along with a fully intercalated region at 14% strain. For mSBR23-20A, shear was successful in reducing the amount of time needed to achieve a fully intercalated sample as compared to static intercalation.

The same experiment was completed with mSBR23 and 93A clay resulting in similar results. mSBR23-93A was sheared for 4 hours. Figure 3.6 shows that at t = 4 hours under static conditions, mSBR23 has not begun intercalation and

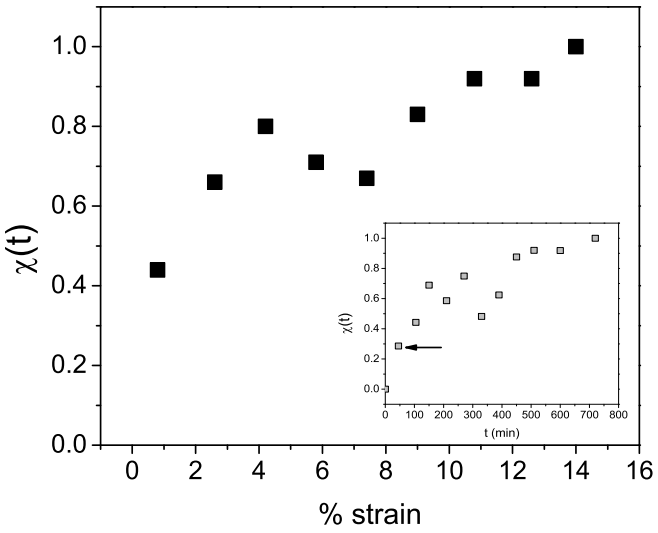

Figure 3.8: Fraction of intercalated 20A clay as a function of strain. For reference, the inset shows fraction of intercalated clay as a function of time. The arrow in the inset represents the amount of time shear was applied to this particular sample. The intercalation behavior is gradual both as a function of time and as a function of strain. At t = 30minutes, 20A clay is ~ 30% intercalated statically, but at the same amount of time with shear, a fully intercalated hybrid can be achieved.

does not begin to intercalate 93A until 400 minutes (over 6.5 hours). Figure 3.9 shows SAXS spectra for mSBR23-93A at various points along the pellet. At 17% strain and less, clay is completely unintercalated. At 17.4% strain, clay is approximately 67% intercalated, and at 18.6% strain, the clay is fully intercalated. Thus, full intercalation was reached with shear at anneal times less what is needed to begin intercalation in static conditions. The fraction of intercalated clay calculated from these spectra is plotted in Figure 3.10 as a function of strain. The intercalation behavior of 93A is much more abrupt as function of strain compared to 20A. Small differences in the amount of strain make the difference between completely unintercalated and completely intercalated clay. This abrupt behavior is similar to the intercalation fraction as a function of time (see inset or Figure 3.6). Intercalation takes a long time to begin (lag time), but once it has started, full intercalation is reached in less time than it takes to fully

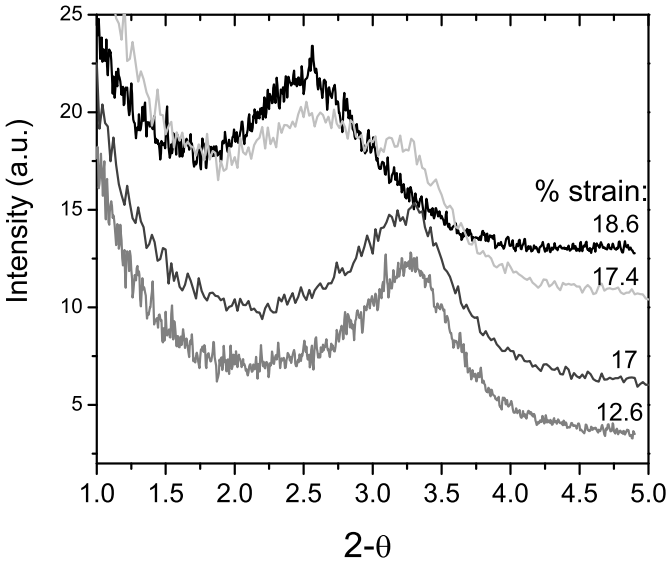

Figure 3.9: SAXS diffraction spectra for mSBR23 with 93A at different amounts of strain. Regions of more strain are further intercalated than regions with less strain.

intercalate 20A.

A final experiment with mSBR23 and Cloisite 10A was tested. 10A is modified with a di-methyl benzyl hydrogenated tallow ammonium and does not intercalate mSBR23 under static conditions (annealed for 3 days until thermal decomposition of the clay). SBR23-10A was sheared for 16 hours, an arbitrary amount of time. After that amount of time, no intercalation was observed. It is unlikely that shear induces intercalation of a clay that is not intercalated under static conditions. Shear can, however, better disperse clay particles or decrease shear viscosity such that polymer transport to the particles is quicker.

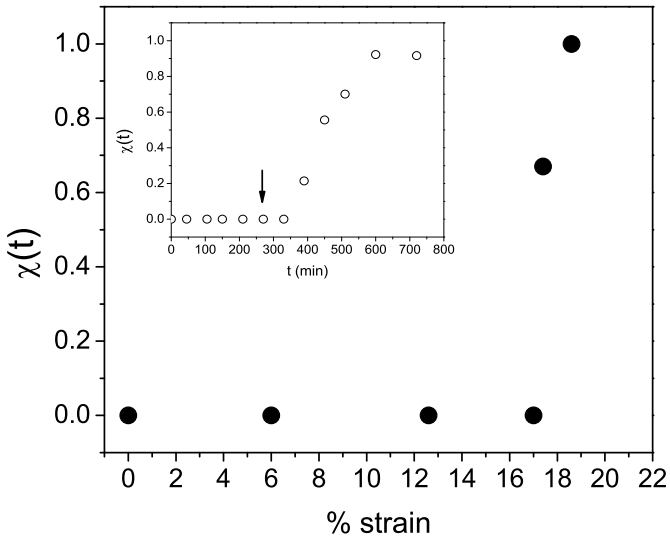

Figure 3.10: Fraction of intercalated 93A clay as a function of strain. For reference, the inset shows fraction of intercalated clay as a function of time. The arrow in the inset represents the amount of time shear was applied to this particular sample. The intercalation behavior is abrupt both as a function of time and as a function of strain. At t = 4 hours, 93A clay is unintercalated statically, but at the same amount of time with shear, a fully intercalated hybrid can be achieved.

3.4 Summary

Intercalation kinetics were measured with x-ray diffraction for various copolymer-clay nanocomposites. Styrene content in SBR copolymer greatly reduces the time needed for intercalation compared to polybutadiene homopolymer. While the differences in diffusivities are dramatic comparing PB to SBR5 and SBR5 to SBR23, the increases in diffusivities slows beyond 20% styrene. As the styrene concentration increases, the number of favorable polymer-clay interactions increases but so does the friction. Intercalation kinetics are a function of both factors, and the plateau effect is due to the balancing of these factors. This effect is observed for both 20A and 93A clays even though 93A has fewer accessible sites with which styrene can interact.

The static intercalation kinetic results were compared to dielectric polymer relaxations of the same nanocomposites. Large diffusivities corresponded well to larger interfacial glass transition temperatures for random SBR copolymers. This was particularly true at lower styrene concentration SBRs where the influence of friction was lower. The correlation between D_{eff} and T_{gi} does not hold as well for SBR block copolymer where the copolymer architecture greatly changes the intercalation behavior. The static intercalation kinetics results were also compared to SBR nanocomposites that had been sheared. Composites that experienced a lag time before static intercalation also experienced a lag with shear (i.e. small amounts of strain do not induce intercalation while large amounts do). Regardless, at the same temperature and for the same amount of time of static anneal versus shearing, the sheared samples were further intercalated compared to the static annealed samples. Shear could not induce intercalation in samples that were not intercalated statically.

BIBLIOGRAPHY

[1] Vaia, R.; Jandt, K.; Kramer, E.; Giannelis, E. *Macromolecules* **1995**, *28*, 8080–8085.

[2] Manias, E.; Chen, H.; Krishnamoorti, R.; Genzer, J.; Kramer, E.; Giannelis, E. *Macromolecules* **2000**, *33*, 7955–7966.

[3] Dennis, H.; Hunter, D.; Chang, D.; Kim, S.; White, J.; Cho, J.; Paul, D. *Polymer* **2001**, *42*, 9513–9522.

[4] Wu, D.; Zhou, C.; Zhang, M. *J. Appl. Polym. Sci.* **2007**, *105*, 1740–1748.

[5] Wu, D.; Zhou, C.; Zheng, H. *J. Appl. Polym. Sci.* **2006**, *99*, 1865–1871.

[6] Chen, H. Ph.D. thesis, Cornell University, 2001.

[7] Wu, D.; Sun, Y.; Zhang, M. *J. Polym. Sci. Part B: Polym. Phys.* **2009**, *47*, 608–618.

[8] Li, J.; Zhou, C.; Zhao, D. *J. Appl. Poly. Sci.* **2003**, *89*, 318–323.

[9] Kong, D.; Park, C. *Chem. Mater.* **2003**, *15*, 419–424.

[10] Fleischer, G.; Appel, M. *Macromolecules* **1995**, *28*, 7281–7283.

[11] Valignat, M.; Oshanin, G.; Vilette, S.; Cazabat, A.; Morceau, M. *Phys. Rev. Lett.* **1998**, *80*, 5377–5380.

CHAPTER 4

COMPATIBILIZING POLY(VINYLIDENE FLUORIDE)/NYLON-6 BLENDS WITH NANOCLAY

4.1 Introduction

[1] Poly(vinylidene fluoride) (PVDF) is a semicrystalline engineering polymer with very good resistance to chemicals, oxidation, and UV radiation. However, it suffers from low strength and ductility. Nylon 6 (N6), another semicrystalline engineering thermoplastic, is very ductile and has good mechanical properties, but it is prone to water absorption and has poor resistance to thermal oxidation and UV radiation. An intuitive way to optimize the properties of these two polymers is to blend them. To that end, Liu et al. have studied PVDF/N6 blends of different compositions and have found that the polymers can have favorable molecular interactions compared to other immiscible polymer blends [1]. Despite the interaction though, PVDF/N6 blends are immiscible over the entire concentration range. To change the interface and improve the miscibility, researchers have attempted several methods of compatibilization including grafting a co-polymer onto N6 which is compatible with PVDF [2] and complexation of N6 amide groups with zinc cations grafted onto PVDF [3].

In this study, we use inorganic nanoparticles as an alternative means to control interfacial properties. Nanoclays are an attractive alternative to traditional compatibilizers because they can be inexpensive, easily melt compounded with polymers, and non-polymer specific potentially compatibilizing many different

[1] Reproduced in part with permission from Vo, L.T.; Giannelis, E.P. *Macromolecules* **2007**, 40, 8271-8276. Copyright 2007 American Chemical Society.

polymer blends. Nanoclays have also been shown to enhance the mechanical and thermal properties and stabilize different crystalline phases of a polymer [4, 5].

A few polymer blend/clay nanocomposite systems have already been studied [6, 7, 8, 9, 10, 11, 12, 13, 14, 15]. Some of these systems exhibit finer morphology and improved interfacial adhesion [6, 7, 8, 9]. Unfortunately, the polymer blend nanocomposites share the same trade-offs as traditional polymer composites and some polymer nanocomposites: while the composites become stiffer, they also become less tough [6, 7]. We report here a polymer blend/clay system with increases in stiffness, strength, and toughness. Furthermore, our studies using different clays as well as sequential compounding (i.e. incorporating the clay into one polymer before blending with the second polymer) reveal a trend that suggests toughness is related to the domain size and degree of crystallinity of the domain phase. The domain size is controlled by the PVDF/N6 viscosity ratio and interfacial tension which are ultimately determined from the surface modification of the nanoclay and the dispersion of the nanoclay particles.

4.2 Experimental Part

N6 (1022B) pellets were provided by UBE Industries, ground to 2mm particles, and dried at 80°C under vacuum for 12 hours. PVDF (Kynar 721) was provided by Arkema and modified montmorillonite clays (Cloisite 30B and Cloisite 20A) were obtained from Southern Clay Products. Both were used as received. For the one batch samples, PVDF/N6 powders were combined with the appropriate amount of clay in a speed mixer. The mixture was extruded at 240°C under

flowing nitrogen for 5 minutes using a DSM twin screw microcompounder. For the sequential studies, clay was first extruded with one polymer. The resulting composite was then ground to 2mm particles and extruded with the second polymer of the blend. The amount of clay in the sequence blends was 4.76% by weight (PVDF/N6/clay 30:70:5) after blending. When studying blends with different clays, the weight percent of silicate in the blends was held constant (3.3%). To mold dog-bone shaped samples (ISO 527-2-5A standard) for tensile testing, a microinjector was used with the barrel at 275°C, the mold at 110°C, and the injection pressure at 110psi.

Blend morphology was examined using a Leo 1550 Keck Field Emission SEM and a Technai T12 TEM operating at an accelerating voltage of 120kV. Samples for the SEM were fractured under liquid nitrogen and then coated with Au/Pd. Samples for TEM were sectioned from molded dogbones to 70nm at −60°C using a diamond knife. For PVDF/N6 30:70 blends, the greater electron density of PVDF domains was sufficient to provide contrast in the TEM. For the inverse blends PVDF/N6 70:30, N6 domains were stained with phosphotungstic acid. The microtomed sections were exposed to a 2% aqueous solution of the acid for 30 minutes. Domain size was determined using ImageJ processing program on several images ranging from 20kx to 50kx magnification. Diffraction spectra were collected on a Scintag Inc. $\theta - \theta$ diffractometer with a CuKα source (λ = 1.54Å) and a germanium detector, scanning at 3°min^{-1}. Degree of crystallinity was evaluated by following the equations outlined previously[4, 16] and using a TA instruments Q1000 DSC scanning 10°C/min from ambient temperature to 250°C; a heat/cool/heat cycle was used to eliminate any thermal history in the extruded material. Thermomechanical properties were obtained from a TA Instruments DMA 2980 scanning from −70°C to 200°C operating

at 1Hz. Mechanical properties were determined using an Instron 5569 tensile tester at an extension rate of 5mm/min (strain rate of 18%/min). Five dogbone specimens were tested for each sample. The standard deviations were within 10% of the average values of the tensile properties. Rheological measurements were made using a MCR 300 under nitrogen flow at 240°C in oscillatory shear configuration with a 1% strain.

4.3 Results

4.3.1 Homopolymers with clay

To aid determining the role of the clays in the blend, the effect of the clays on each polymer must be first ascertained. The clay nanoparticles used in this work were modified via cation exchange with quaternary ammonium cations to render the clay surface more organophilic. The differences in the functional groups of the cations offer varying affinities to the polymers such that the location of the clay can be tuned to optimize blend properties. Cloisite 30B (herein referred to as 30B) is modified with bis(2-hydroxyethyl) tallow alkyl ammonium and interacts more favorably with the polar amide group of N6. In N6, the clay is well dispersed (exfoliated), whereas it is intercalated in PVDF (Figure 4.1a). Cloisite 20A (herein referred to as 20A), modified with dimethyl dehydrogenated tallow alkyl ammonium, is less polar than 30B and interacts comparably with the two polymers; both PVDF and N6 intercalate 20A (Figure 4.1b).

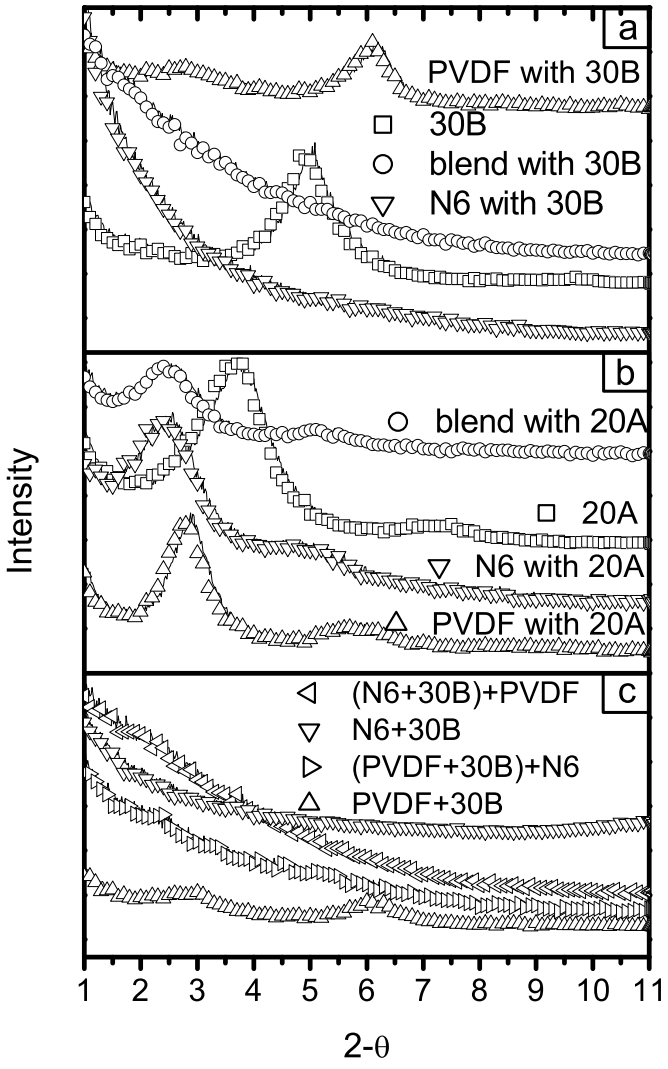

Figure 4.1: XRD plots for (a) 30B, PVDF with 5% 30B, N6 with 5% 30B, and PVDF:N6 30:70 blend with 5% 30B. 30B is intercalated by PVDF and exfoliated by N6 and PVDF:N6 30:70 blend. (b) 20A, PVDF with 5% 20A, N6 with 5% 20A, and PVDF:N6 30:70 blend with 5% 20A. 20A is intercalated by PVDF, N6, and PVDF-N6 blend. (c) N6+30B and PVDF+30B after first step in sequential blending. 30B is exfoliated by N6 and intercalated by PVDF. The blends created the after second step is also shown in (c). The clay in (N6/30B)/PVDF) blend is exfoliated, while the clay in (PVDF/30B)/N6 still retains some regular layering.

4.3.2 One batch blend with Cloisite 30B

Given that N6 disperses one of the clays, N6 was chosen to be the matrix phase (70%) and PVDF to be the domain phase (30%) for the majority of this work. (The case of inverted blend composition is covered in Section 4.3.5). As expected from the known immiscibility of PVDF and N6, PVDF forms domains in the N6 matrix at a ratio of 30:70 PVDF:N6. The size of the largest domains is approximately 150nm as determined from TEM and SEM imaging (Figure 4.2a,c). (In the TEM micrograph, dark zones represent PVDF domains). In comparison, the morphology of the blend with 5% 30B clay is finer and more uniform with the largest domains being 60nm (Figure 4.2b). The domain sizes and size distribution was determined using an image analysis program. The distribution plot is shown in Figure 4.3.

The location of the clay nanoparticles was also investigated by TEM and SEM (Figure 4.2b,d). The TEM micrograph (Figure 4.2b) shows the majority of the clay dispersed in the N6 matrix. XRD patterns (Figure 4.1a) confirm the disordered (exfoliated) structure as the nanocomposite blend did not possess a characteristic peak indicative of layered clays. The TEM micrograph also shows some of the clay at the PVDF/N6 interface. The SEM micrograph of the fracture surface of this blend nanocomposite (Figure 4.2d) supports the improvement in the interfacial adhesion as the blend nanocomposite has fewer visible domains compared to the blend and shows practically no debonding.

The presence of clay simultaneously in the bulk and the interface is atypical. Previous studies of polymer blend/clay systems usually show the clay either residing at the interface [6, 9, 12] or in the bulk [7, 14]. This dual positioning indicates two roles for the nanoclay particles: one as a compatibilizer with the

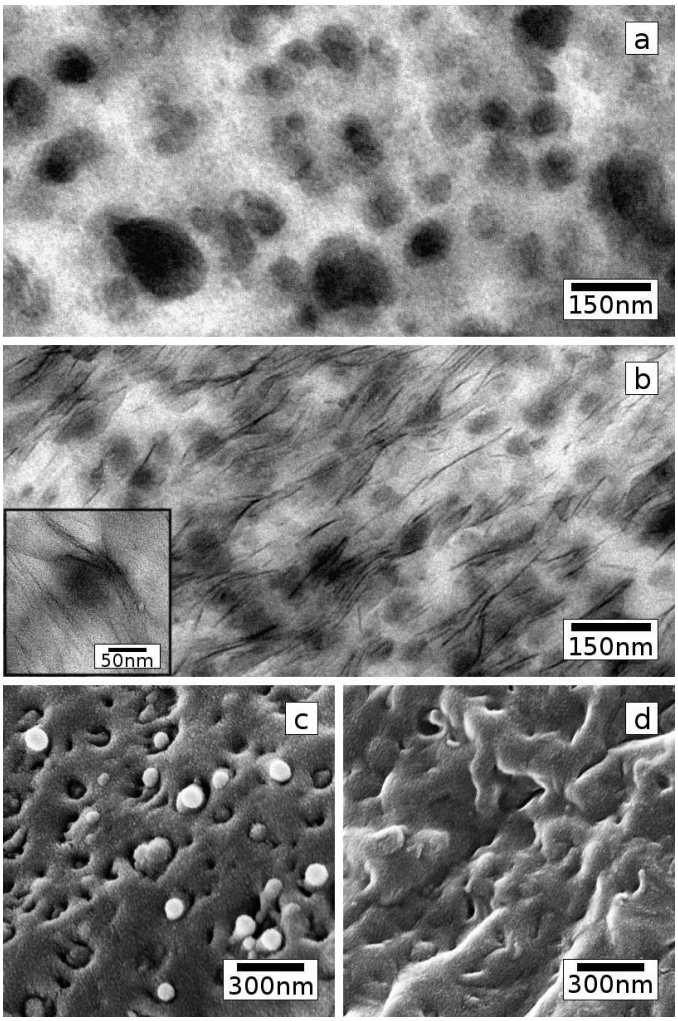

Figure 4.2: TEM micrographs of a) PVDF/N6 30:70 blend and b) 30:70 blend with 5% 30B. The PVDF domains in the blend vary in size, while the domains in the blend nanocomposite are smaller and more uniform in size. Clay is well dispersed in the matrix and is also located by the domains. Inset in (b) shows some clay residing the PVDF/N6 interface. This figure also shows SEM micrographs of fracture surfaces of c) PVDF/N6 30:70 blend and d) blend with 5% 30B. The fracture surface of the blend breaks cleanly along the PVDF-N6 interface showing visible PVDF domains, while the fracture surface of the blend nanocomposite is rough and shows fewer visible domains.

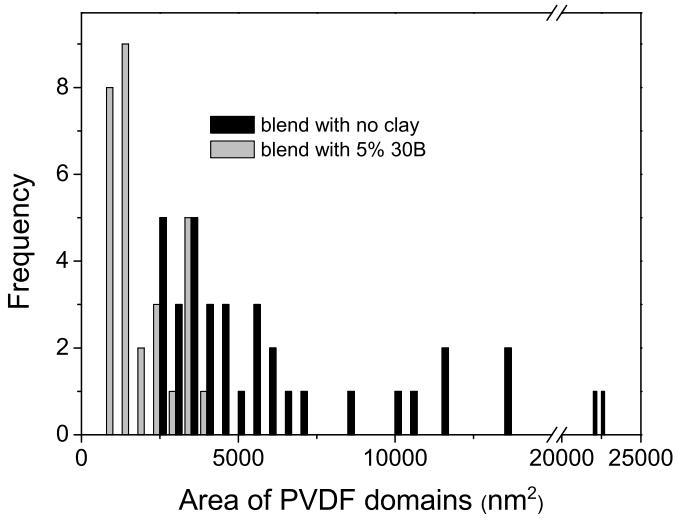

Figure 4.3: Size distribution of PVDF/N6 30:70 blend and blend with clay as calculated from TEM images. There are large domains in the blend and the domain size distribution is wide. In the blend nanocomposite, the domain sizes are smaller and the size distribution is more narrow.

clay being shared by both polymers and the other as a nanofiller, stabilizing a different polymer crystalline phase and improving the mechanical properties as will be discussed in the following paragraphs.

Since 30B interacts favorably with N6, it is expected that the polymer would display the same polymorphism behavior as previously observed in nylon nanocomposites [5, 16, 17]. N6 has two stable crystalline phases, α and γ. Injection molded N6 consists of a mixture of α and γ phases, but upon clay addition N6 preferentially forms the γ phase. From the wide angle XRD patterns (Figure 4.4) and DSC melting thermographs of the blends (Figure 4.5a), N6 in the blends experiences the same crystal phase transformation when compounded with clay. In the blend with no clay, N6 exists mainly in the α-form, but with increasing clay concentration, the ratio of α to γ phase decreases with the 5% clay blend consisting mainly of γ phase. (In Figure 4.4, the diffraction peaks at $2\theta = 19.5^\circ, 23.5^\circ$ correspond to the α-phase while that at $2\theta = 21^\circ$ corresponds

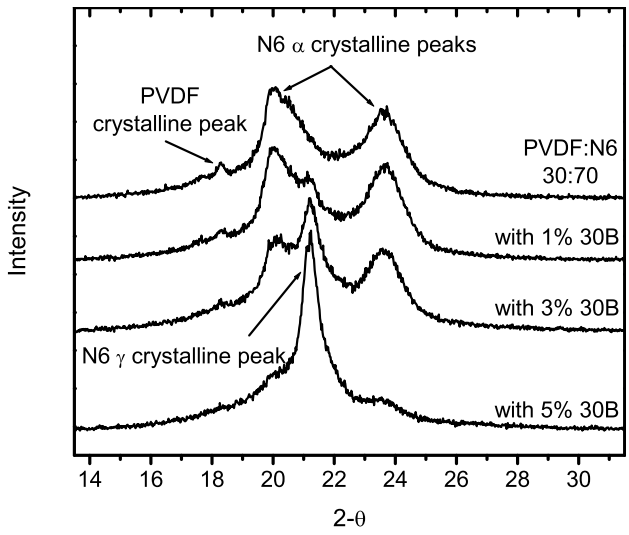

Figure 4.4: WAXS plots of the PVDF/N6 30:70 blend and blends with various concentrations of 30B. N6 in the blend exists in the α-crystalline form. With increasing clay concentration in the blend, the ratio of α to γ crystalline form decreases with 5% clay resulting in a blend with mostly γ N6 crystalline form. The XRD spectra also show the decreasing PVDF crystallinity with increasing clay concentration.

to the γ-phase. In Figure 4.5a, the α-form of N6 melts at 220°C while the γ-form melts at 212°C). In the blend nanocomposite, the clay in the N6 matrix acts as a nucleating agent stabilizing the γ crystalline form of N6 similarly to the clay in the homopolymer[16].

The effect of the clay on PVDF, however, is to hinder crystallization. The PVDF melting peak (at 169°C) shifts to higher temperatures (indicating interaction with clay[4, 18]) and decreases in area as the amount of clay increases (Figure 4.5a). In addition, the T_c and T_g peaks of PVDF are also suppressed as observed by DSC (not shown) and DMA (Figure 4.6), respectively. The crystallization and glass transition suppression is due to the restricted movement of the PVDF. Not only is the PVDF in smaller domains (such that the PVDF properties are no longer dominated by the larger more bulk-like domains), but the PVDF chains are constrained by clay platelets surrounding the domains. Other

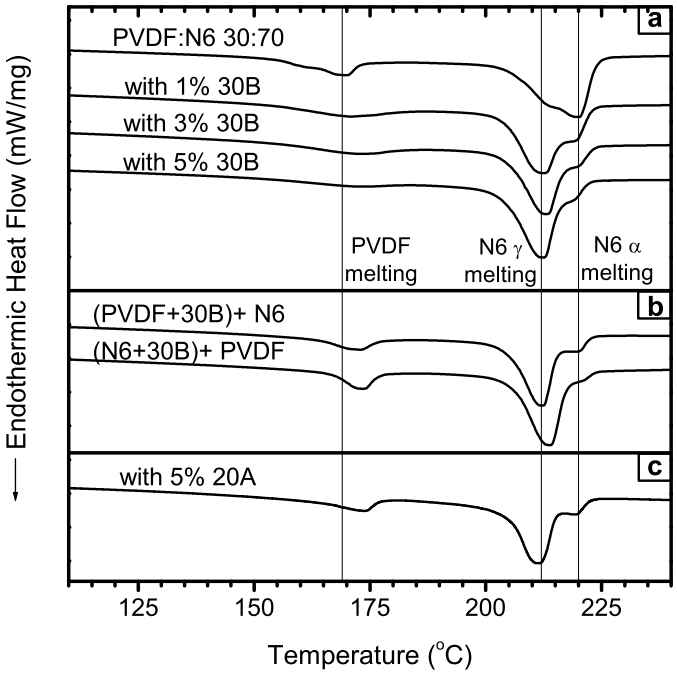

Figure 4.5: DSC melting curves for (a) PVDF/N6 30:70 blend and blends with various concentrations of 30B. With increasing clay concentration, the crystalline form of N6 shifts from α to γ crystalline form. With increasing clay concentration, PVDF also becomes less and less crystalline. (b) sequential 30B blends. PVDF domains in both sequential blends are somewhat crystalline, with the PVDF domains in the (N6+30B)+PVDF blend being more crystalline. (c) one batch 20A blend. PVDF in a blend with N6 and 20A clay is also somewhat crystalline.

studies with confined polymers have also shown suppressed thermal transitions [13, 19, 20, 21, 22]. For example, Nakajima et al. [19] found that polypropylene confined in mesoporous silica does not exhibit a crystalline melting point, and Jiang et al [20] saw the same with polyethylene oxide confined in organic networks.

One of the ultimate purposes for polymer blending and compatibilizing is to improve mechanical properties. If in fact there is compatibilization, the blend should exhibit improved mechanical properties. Figure 4.7a shows a representative stress/strain curve for the blend and the blend with 1 and 5% clay. With

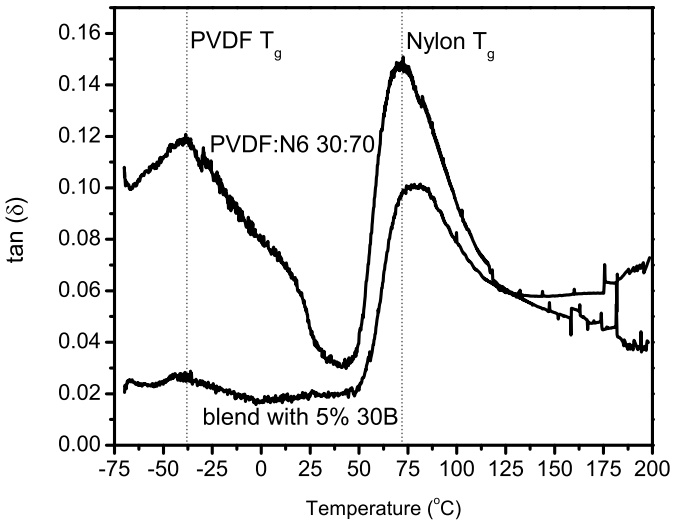

Figure 4.6: DMA tan(δ) curves showing the glass transition temperatures of PVDF and N6 for the blend and blend with 30B clay. The glass transition temperature of N6 is virtually unchanged, but the glass transition for PVDF is suppressed.

as little as 1% clay, the tensile properties of the blend nanocomposite are improved compared to the blend without clay. The blend with 5% clay is even stronger and tougher. Not only are the blend nanocomposites stiffer (with a modulus of E = 2.68 ± 0.05GPa for the 5% blend compared to 1.90 ± 0.04GPa for the blend without clay), they also show higher elongation and strength. For the 5% clay blend, these improvements translate to ≈ 170% increase in toughness (defined as the area under a stress/strain plot). For comparison, the stress-strain curves of the homopolymers and their nanocomposites are shown in Figure 4.7b. The 30B blend nanocomposite also has higher yield and ultimate stresses and is stiffer than PVDF (E = 1.31 ± 0.06GPa), the PVDF nanocomposite (E = 1.36 ± 0.04GPa), N6 (E = 1.67 ± 0.09GPa), and the N6 nanocomposite (E = 2.40 ± 0.12GPa).

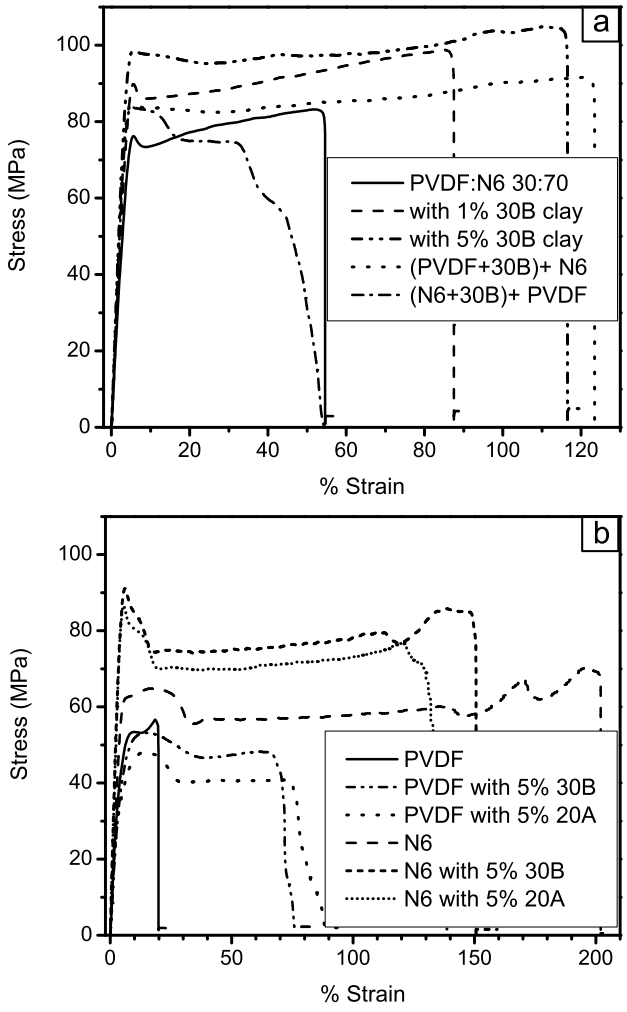

Figure 4.7: Tensile stress-strain curves for (a) blend and 30B modified blends. The one batch blends and (PVDF+30B)+N6 sequential blend are much tougher (stiffer, strong, and more ductile) than the blend without clay. (N6+30B)+PVDF sequential blend has comparable properties to the blend without clay. (b) the homopolymers and their nanocomposites. N6 homopolymer is very ductile; its nanocomposites are also very ductile but are stronger and stiffer than the homopolymer.

4.3.3 Sequential compounded blends with Cloisite 30B

For the blends in the previous section, the clay nanoparticles were blended with both polymers simultaneously. To better understand the kinetics of nanoparticle diffusion on blend properties, a series of experiments were performed where the 30B clay was first compounded with one polymer and then the resulting composite was compounded with the second polymer. The 30B clay interacts more favorably with N6, so in the blend in which PVDF is blended with 30B first and then with N6 (referred to as (PVDF/30B)/N6), it is expected that 30B will migrate to the interface and/or the matrix. For the inverse sequence blend in which 30B is compounded first with N6 and then with PVDF (referred to as (N6/30B)/PVDF), it is expected that the 30B nanoparticles will more likely reside in the matrix.

To assess the evolution of the clay dispersion, XRD patterns were obtained after the first sequence step and again after the blends were fully compounded (Figure 4.1c). As expected, 30B compounded with N6 is exfoliated as is the (N6/30B)/PVDF blend. For the inverse sequential blend, 30B compounded only with PVDF is intercalated. When this PVDF/clay composite is compounded with N6, the blend has traces of intercalated clay but appears to be mostly exfoliated. The DSC melting curve of this sequential blend, (PVDF/30B)/N6, confirms the migration of clay from PVDF to N6 as the N6 γ crystalline phase, the phase typically present in N6 nanocomposites, is the dominant phase. However the ratio of N6 α to γ-phase of the (PVDF/30B)/N6 blend is larger than the ratio for the (N6/30B)/PVDF blend indicating incomplete migration of clay from the PVDF.

TEM images support the overall exfoliation of clay in N6 for both blends

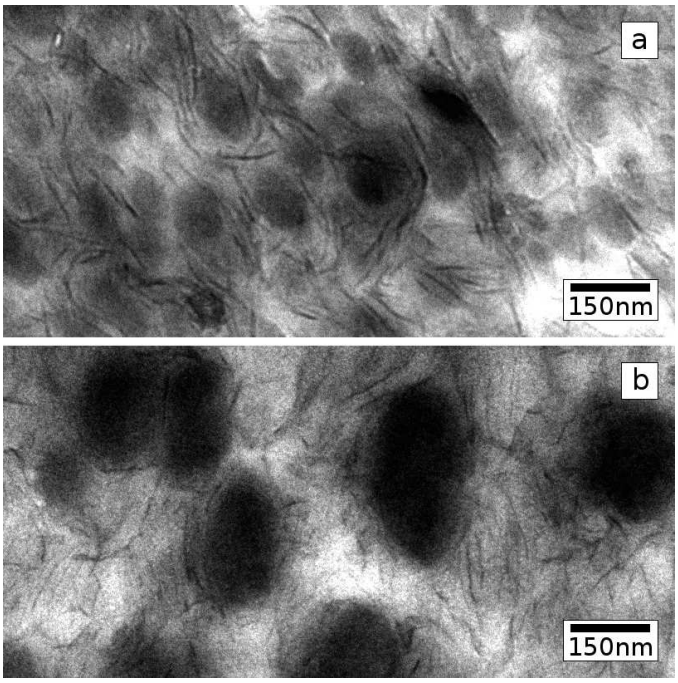

Figure 4.8: TEM micrographs of PVDF/N6 30:70 blend nanocomposites with 5% 30B in which a) clay was compounded first with PVDF [(PVDF/30B)/N6] and b) clay was compounded first with N6 [(N6/30B)/PVDF]. The domain sizes in (a) blend nanocomposite are much smaller than (b) blend nanocomposite. The clay nanoparticles appear to be well dispersed in both samples.

(Figure 4.8). Comparison of the TEM images with each other as well as to the image of the one batch blend (Figure 4.2b) shows a striking difference among the blends' domain sizes. The PVDF domains in the (PVDF/30B)/N6 blend are approximately 110nm; the domains are not as small as the one batch blend (~ 60nm) but not as large as the domains of the blend with no clay (~ 150nm). However, the (N6/30B)/PVDF sequential blend exhibits larger domains (~ 240nm) than the blend with no clay. The reasoning for this discrepancy will be addressed in a later section.

In addition to different domain sizes, the amount of PVDF crystallization in the two sequential blends is also different. Unlike the one batch blend with 5% 30B, the PVDF in the sequential blends experiences little or no crystallization

suppression. PVDF in the (PVDF/clay)/N6 blend is 24% crystalline, and it is 33% crystalline in the (N6/clay)/PVDF blend. Comparison of the domain size to the PVDF percent crystallinity indicates that smaller domains correlate to less crystalline domains.

Due to the larger domain size and lack of crystallization suppression in the sequence blends, the mechanical properties of the sequential blends were poorer than those of the one batch blend (Figure 4.7a). The (N6/clay)/PVDF sequence blend with large domains is stiff (E = 2.52 ± 0.06GPa) but showed no improvement in toughness or strength compared to the blend with no clay. Conversely, the (PVDF/clay)/N6 blend is stiffer (E = 2.59 ± 0.04GPa), stronger, and tougher compared to the blend with no clay but was inferior to the one batch 30B blend.

4.3.4 One batch blend with 20A

While the 30B clay interacts favorably with both polymers, it prefers more the N6 and hence is more likely to be dispersed in the matrix. To study the effect of clay location on the blend, a less polar clay, 20A, was chosen for blending. The 20A particles interact comparably with the polymers and are more likely to reside at the interface than the 30B particles.

The blend nanocomposite of PVDF/N6 30:70 with 20A clay shows an intercalated structure (Figure 4.1b). Since both polymers intercalate to approximately the same d-spacing, it cannot be distinguished which one is intercalating the clay. The DSC curve of the blend (Figure 4.5c) shows both a shift of PVDF melting to higher temperatures and a shift of N6 melting to predominantly γ-phase indicating that both polymers are interacting with the clay. It is possible

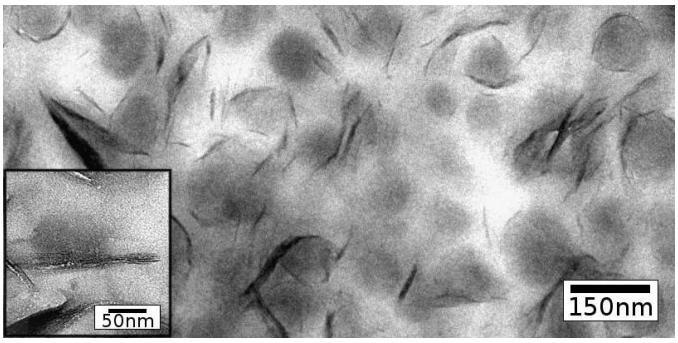

Figure 4.9: TEM micrograph of PVDF/N6 30:70 blend with 5% 20A. Inset shows an intercalated clay structure at the PVDF/N6 interface.

that they both intercalate the clay but not in the same gallery[8].

TEM images of the blend nanocomposite with 20A clay indicate that the intercalated clay layers are located primarily at the interface interacting with both PVDF and N6 (Figure 4.9). The images also show the average size of the PVDF domains as being approximately 120nm, but unlike the 30B blends, the PVDF domain size for the 20A blend is highly varied ranging from 70 to 150nm.

The inhomogeneity of domain sizes translated to differing toughness for the 20A blend nanocomposites (Figure 4.10). Some blend samples strain hardened and were comparable in elongation to the 30B samples. Other samples failed to strain harden and fractured prematurely, and some fractured somewhere in between. There was not enough statistical consistency despite efforts to improve the processing conditions. Since there was a correlation between PVDF crystallinity and toughness in 30B based nanocomposite blends, DSC measurements were performed on the 20A dogbone specimens at the point of fracture to assess the crystallinity. Indeed PVDF in high strain fractured samples was ~25% less crystalline than the PVDF in samples that fractured early, reinforcing the idea that crystallization suppression of PVDF is vital to blend toughening. Compare the PVDF percent crystallinity of the low strain 20A blend (X_C = 34%)

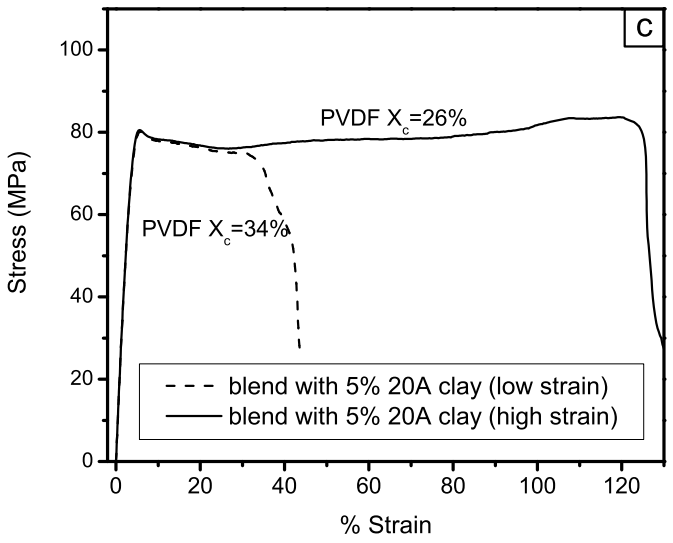

Figure 4.10: Tensile stress-strain curves for 20A modified blend. The mechanical properties of the blend with 20A are varied. Some samples are very ductile compared to the blend (Figure 4.7a), but some have comparable properties to the blend.

and the high strain 20A blend (X_C = 26%) to the blend with no clay (X_C = 29%) and the sequential blend nanocomposites [X_C = 24% for (PVDF/30B)/N6 and X_C = 33% for (N6/30B)/PVDF].

4.3.5 Blends at inverted composition

While clay preference for N6 indicates that a blend of N6 matrix and PVDF domains is the most logical, this section explores the effect of the inverse blend. The inverted blend has PVDF and N6 mixed in a ratio of 30:70, respectively, with 30B clay. The inverted blend offers extreme variables in the opposite direction allowing for study of how each variable plays a role in blend morphology and compatibilization.

In a blend with 30% N6 and 70% PVDF, N6 forms very large domain of

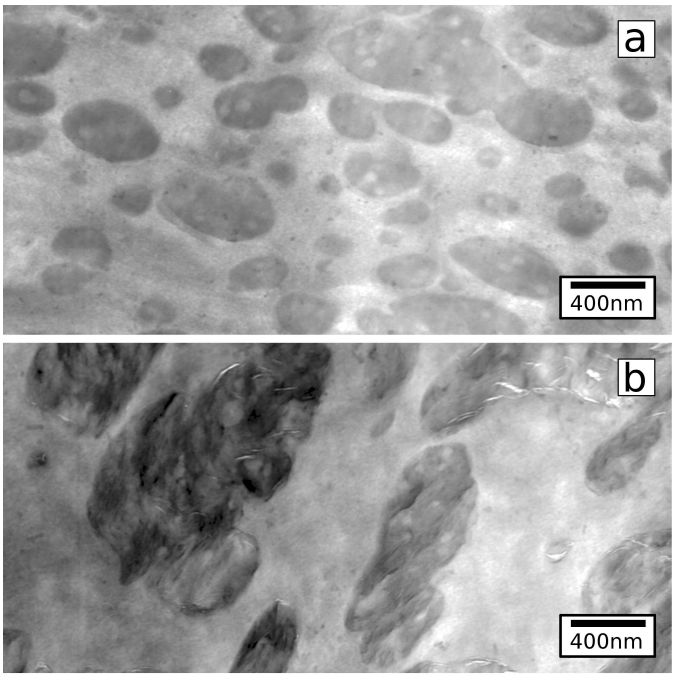

Figure 4.11: TEM micrographs of a) PVDF/N6 70:30 blend and b) 70:30 blend with 5% 30B. The N6 domains in the blend vary in size and are much larger than PVDF domains at the inverse composition. The N6 domains in the blend nanocomposite are much larger than in the blend. Clay nanoparticles appear to preferentially reside in the N6 domains.

~ 450 nm as determined from TEM imaging (Figure 4.11a). When 30B clay is added to this blend, the N6 domains are even larger at ~ 700 nm (Figure 4.11b). Figure 4.11b also shows the location of clay nanoparticles. Since clay prefers N6, it is not surprising that clay is located mostly within the domains. The clay is spread througout the domains including at the interface. XRD of the blend nanocomposites indicates an exfoliated clay structure (Figure 4.12); since N6 exfoliates the clay while PVDF intercalates it, this is in line with TEM imaging of clay location.

The preference of clay for the domains affects the crystalline structure of the blend differently from the previous cases. Whereas in the previous cases (with the inverse blend composition), the domain crystallinity was suppressed,

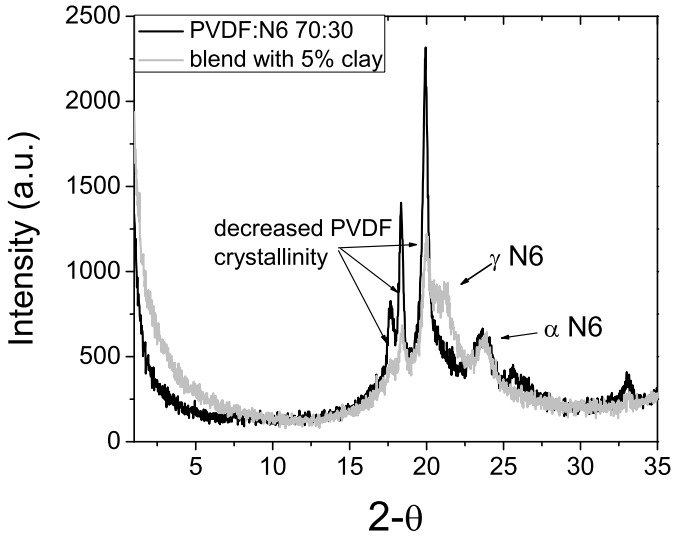

Figure 4.12: XRD of PVDF/N6 70:30 blend and blend with 5% 30B clay. Clay nanoparticles in both in the blend and blend nanocomposite are exfoliated. In the blend, PVDF is comprised of α-crystalline phase, and N6 is comprised of α-crystalline phase. In the blend nanocomposite, PVDF is less crystalline compared to the blend, and N6 is comprised of a mixture of α and γ crystalline phases.

in this case, the domain (N6) crystallization is enhanced. DSC scans comparing the blend to blend with clay (Figure 4.13) show that in the blend with clay, the peak associated with N6 melting is larger (34% crystalline) than in the blend alone (18% crystalline). Clay is known to enhance crystallization, and with clay in the domains, the domains are more crystalline. There is also a shift from α-crystalline form to γ-crystalline form as evidence by both DSC (Figure 4.13) and wide angle x-ray (Figure 4.12). However, the peak associated with PVDF melting in the nancomposite is smaller (41% crystalline) than in the blend (50% crystalline). In this case, crystallinity is not perturbed as much by clay presence as by the much larger domains of N6. In the presence of 30B, homopolymer PVDF crystals change from α-phase to β-phase[23]. The α-phase is characterized in XRD at $2\theta = 17.2°, 17.9°, 19.5°$, and β-phase at $2\theta = 18.3°, 19.9°$. In

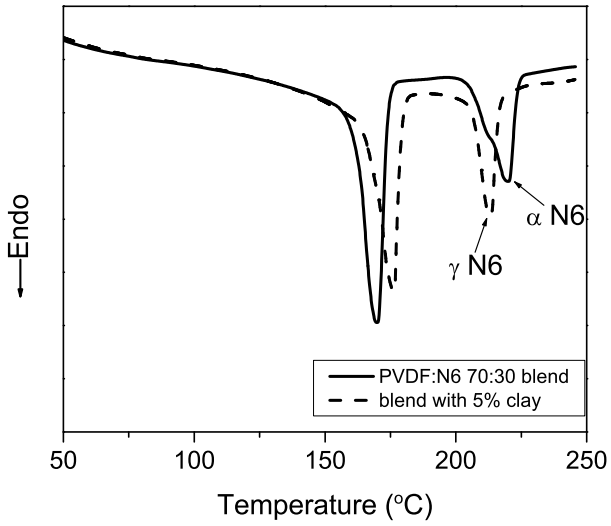

Figure 4.13: DSC melting curves for PVDF/N6 70:30 blend and blend with 5% 30B clay

this case though the wide angle x-ray diffraction pattern (Figure 4.12) for the blend nanocomposite shows PVDF α-phase peaks indicating little interaction between the clay and PVDF. Compared to the PVDF peaks of the blend (no clay), the peaks of the blend with clay are reduced in intensity confirming DSC scans showing decreased PVDF crystallinity in the nanocomposite.

The localization of clay, large domain sizes, and enhanced domain crystallinity translate to poor mechanical properties (Figure 4.14). The blend nanocomposite is stiffer (E = 1.9GPa) and stronger (σ_f = 73MPa) compared to the blend (with modulus and final stress of 1.3GPa and 64MPa, respectively). However, the nanocomposite is less ductile breaking at 10% strain compared to 16% strain. Due to the large initial domain size (before clay addition) as well incompatible domain mechanical properties compared to the matrix, these blends are worse overall than the PVDF/N6 30:70 blends with or without clay.

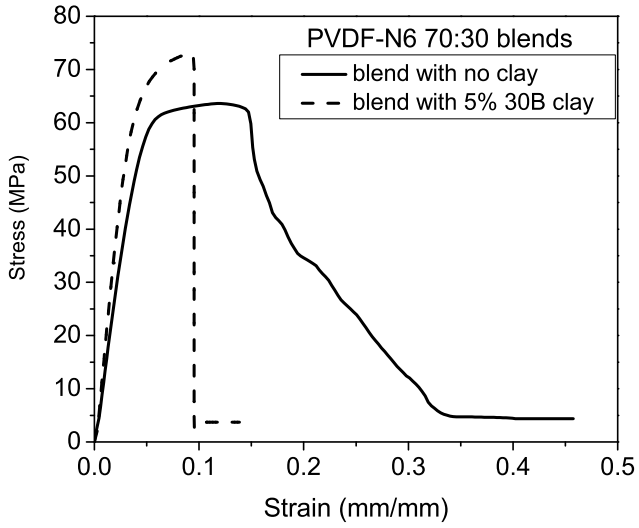

Figure 4.14: Tensile stress-strain curves for PVDF/N6 70:30 blend and blend with 5% 30B. The blend nanocomposite is slightly more ductile but less stiff and strong compared to the blend.

4.4 Discussion

The blend nanocomposite that displayed the best compatibilization characteristics is the one batch blend with 5% 30B. In this nanocomposite, the clay prevented the coalescence of the minor phase, stabilized the domain morphology, changed the interfacial properties, and enhanced the blend performance. To some degree these properties were also observed in the (PVDF/30B)/N6 sequence blend and to a lesser extent the blend with 20A. The differences in behavior of these blends offer insight to the overall compatibilization mechanism.

There appears to be a direct link between mechanical toughening and percent crystallinity of the domain phase; tougher blends have less crystalline PVDF domains. The one batch 5% 30B blend was the toughest, and the (PVDF/30B)/N6 sequence blend and 20A blend samples with suppressed crys-

tallinity in the tensile region also displayed large strains to failure. On the other hand, the (N6/30B)/PVDF sequence blend nanocomposite and the 20A blend samples with no crystallinity suppression were less tough.

Controlling the domain size is crucial as the amount of crystallinity scales with domain size. In a polymer blend, which is essentially a mix of two viscous, incompressible fluids, domain size is related to the break-up of threads (surrounded by matrix) into droplets due to Rayleigh instability[24]. Empirically, domain size (A_n) has been determined to depend on the interfacial tension (γ), the viscosity ratio of the dispersed phase to the matrix phase $\left(\frac{\eta_d}{\eta_m}\right)$, the shear rate (G), and the melt viscosity (η_{me}) as shown in the equation below[25].

$$A_n = \frac{4\left(\frac{\eta_d}{\eta_m}\right)^k \gamma}{G\eta_{me}} \tag{4.1}$$

where $k = 0.84$ for $\frac{\eta_d}{\eta_m} \geq 1$ and $k = -0.84$ for $\frac{\eta_d}{\eta_m} \leq 1$. The equation implies (and other experimental studies have shown[26]) that the smallest domains are generally the result of a viscosity ratio that is close to unity. For the blends studied in the majority of this work where PVDF is the domain phase and N6 is the matrix phase, the viscosity ratio is less than unity[1]. As long as the ratio is not far from unity, the higher viscosity of the matrix helps break up the less viscous phase and prevent domain coalescence. In the case where N6 is the domain phase and PVDF is the matrix phase, the viscosity ratio is greater than unity. Since the domain phase is the more viscous phase, it is more difficult to break up these droplets under shear. Comparing the domain sizes of the two blends reveals that the domain sizes for PVDF/N6 30:70 are indeed smaller overall than PVDF/N6 70:30.

For the blends in the current study, the shear rate (G) is held constant as the blends are all extruded at the same rate. The viscosity of the blend melt and

the blend with 5% 30B melt are also roughly equal (Figure 4.15), thus the only variables that change with the addition of clay are the viscosity ratio and the interfacial tension. In the (N6/30B)/PVDF sequence blend, it is mainly the viscosity of the N6 matrix phase that is affected because the clay is first mixed with N6 and clay migration from N6 to PVDF is exceedingly slow due to the strong interaction between N6 and 30B. At the extrusion temperature, N6 with 5% 30B is 10 times more viscous than pure N6 in the shear rate range of the extruder. Therefore, in the (N6/30B)/PVDF blend, the viscosity ratio effects $\left(\frac{\eta_d}{\eta_m} \ll 1\right)$ outweigh any changes in the interfacial tension resulting in domains that are larger than the blend with no clay (phase coarsening). However, in the one batch 30B and (PVDF/30B)/N6 blends, the interfacial tension is lowered significantly due to the presence of clay at the PVDF-N6 interface. Even though the viscosity of N6 matrix is still increased in these samples (since 30B is exfoliated in N6), the interfacial tension effects seem to outweigh the viscosity effect resulting in smaller domains for these blends. In the 20A blend nanocomposite, the viscosities for both PVDF and N6 are likely increased as the clay is mostly located at the interface and is probably intercalated by both polymers. If the viscosities of both the matrix and dispersed phases are increased, the viscosity ratio is not as affected by the addition of clay. Thus, in the 20A blend nanocomposite, the interfacial tension effect also seems to outweigh the viscosity effect. However, in the inverted composition blend, PVDF/N6 70:30, clay is localized in the N6 domains increasing the viscosity of the domain phase while the matrix phase viscosity is unchanged. As such, the viscosity effect $\left(\frac{\eta_d}{\eta_m} \gg 1\right)$ greatly outweighs the reduction in interfacial tension resulting in blend nanocomposite domains that are larger in size than domains in the blend with no clay.

Clay dispersion not only affects the viscosity and interfacial tension (and

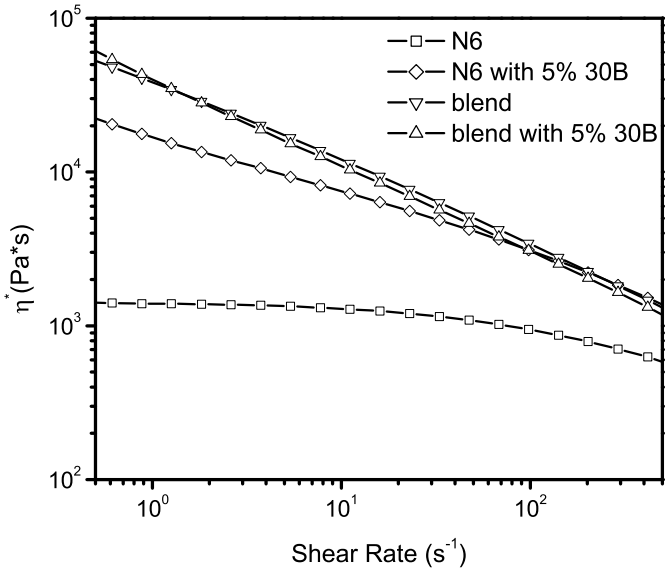

Figure 4.15: Complex viscosity of N6, blend (PVDF:N6 30:70), N6 with 5% 30B, and blend with 5% 30B. The addition of clay greatly increases the viscosity of N6. The viscosity of the blend nanocomposite is virtually unchanged compared to the blend.

thus indirectly contributes to the mechanical properties), it also directly influences the mechanical properties by providing reinforcement. The best properties stem from having the clay well dispersed throughout both the matrix and at the interface. The (PVDF/30B)/N6 sequence blend and 20A blend have good interfacial dispersion, but they suffer from insufficient matrix dispersion. Since the clay was not completely dispersed, both blends were not as strong or stiff as the one batch 30B blends. In addition, the poor dispersion in the 20A samples likely caused the varying domain sizes and premature failure in some samples. Ideally, the compatibilizer nanoparticles should interact favorably with both polymers but prefer the matrix polymer like 30B does with N6.

In the ideal blend nanocomposite, one batch 30B blend, the clay plays two roles which work in tandem to compatibilize the blend. Well dispersed clay in the N6 matrix of the blend stiffens and strengthens the blend similarly to the

clay in the homopolymer. The clay at the interface reduces the interfacial tension resulting in smaller domains with suppressed crystallization. The "amorphous" PVDF domains seem to toughen the blends. We suspect that the domains are acting as rubbery particles in rubber-toughened polymers. In particular, the percent composition of PVDF domains (30%), the low T_g of PVDF ($-40^{\circ}C$), the small size of the domains, and the compliant nature of PVDF compared to N6 are consistent with a rubbery phase in rubber-toughened N6[27, 28]. Further experiments are underway to further elucidate the strengthening/toughening mechanisms. If this is indeed the case and these concepts can be applied more generally to other polymers, nanoparticle compatibilization could potentially be a new method for toughening brittle polymers.

BIBLIOGRAPHY

[1] Liu, Z.; Marechal, P.; Jerome, R. *Polymer* **1998**, *39*, 1779–1785.

[2] Kim, K.; Cho, H.; Yoon, K. *Eur. Polym. J.* **2003**, *39*, 1249–1265.

[3] Mascia, L.; Hashim, K. *Polymer* **1998**, *39*, 369–378.

[4] Priya, L.; Jog, J. *J. Polym. Sci. Part B: Polym. Phys.* **2002**, *40*, 1682–1689.

[5] Liu, L.; Qi, Z.; Zhu, X. *J. Appl. Poly. Sci.* **1999**, *71*, 1133–1138.

[6] Ray, S.; Pouliot, S.; Bousmina, M.; Utracki, L. *Polymer* **2004**, *45*, 8403–8413.

[7] Chow, W.; Ishak, Z.; Ishiaku, U.; Karger-Kocsis, J.; Apostolov, A. *J. Appl. Poly. Sci.* **2004**, *91*, 175–189.

[8] Ray, S.; Bousmina, M. *Macromol. Rapid Commun.* **2005**, *26*, 450–455.

[9] Si, M.; Araki, T.; Ade, H.; Kilcoyne, A.; Fisher, R.; Sokolov, J.; Rafailovich, M. *Macromolecules* **2006**, *39*, 4793–4801.

[10] Dharaiya, D.; Jana, S. *J. Polym. Sci. Part B: Polym. Phys.* **2005**, *43*, 3638–3651.

[11] Gelfer, M.; Song, H.; Liu, L.; Hsiao, B.; Chu, B.; Rafailovich, M.; Si, M.; Zaitsev, V. *J. Polym. Sci. Part B: Polym. Phys.* **2003**, *41*, 44–54.

[12] Voulgaris, D.; Petridis, D. *Polymer* **2002**, *43*, 2213–2218.

[13] Gahleitner, M.; Kretzschmar, B.; Pospiech, D.; Ingolic, E.; Reichelt, N.; Bernreitner, K. *J. Appl. Polym. Sci.* **2006**, *100*, 283–291.

[14] Li, Y.; Shimizu, H. *Polymer* **2004**, *45*, 7381–7388.

[15] Ji, G.; Clement, F.; Giannelis, E. MRS Proceedings, 2001.

[16] Tjong, S.; Bao, S. *J. Polym. Sci. Part B: Polym. Phys.* **2004**, *42*, 2878–2891.

[17] Devaux, E.; S., B.; Achari, A. E. *J. Appl. Poly. Sci.* **2002**, *86*, 2416–2423.

[18] Dillion, D.; Tenneti, K.; Li, C.; Ko, F.; Sics, I.; Hsiao, B. *Polymer* **2006**, *47*, 1678–1688.

[19] Nakajima, H.; Yamada, K.; Iseki, Y.; Hosoda, S.; Hanai, A.; Oumi, Y.; Teranishi, T.; Sano, T. *J. Polym. Sci. Part B: Polym. Phys.* **2003**, *41*, 3324–3332.

[20] Jiang, S.; Qiao, C.; Tian, S.; Xiangling, J.; An, L.; Jiang, B. *Polymer* **2001**, *42*, 5755–5761.

[21] Strawhecker, K.; Manias, E. *Chem. Mater.* **2000**, *12*, 2943–2949.

[22] Vaia, R.; Sauer, B.; Tse, O.; Giannelis, E. *J. Polym. Sci. Part B: Polym. Phys.* **1997**, *35*, 59–67.

[23] Shah, D.; Maiti, P.; Gunn, E.; Schmidt, D.; Jiang, D.; Batt, C.; Giannelis, E. *Adv. Mater.* **2004**, *16*, 1173–1177.

[24] Palierne, J.; Lequeux, F. *J. Non-Newtonian Fluid Mech.* **1991**, *40*, 389–306.

[25] Wu, S. *Polym. Eng. Sci.* **1987**, *27*, 335–343.

[26] Favis, B. Polymer Blends, Vol. 1, New York, NY, 1999; pp 501–537.

[27] Kudva, R.; Keskkula, H.; Paul, D. *Polymer* **2000**, *41*, 225–237.

[28] Okada, O.; Keskkula, H.; Paul, D. *J. Polym. Sci. Part B: Polym. Phys.* **2004**, *42*, 1739–1758.

CHAPTER 5

POLYSTYRENE BLENDS WITH NANOCLAY

5.1 Introduction

Polystyrene (PS) is a commodity polymer with good processing characteristics and stiffness. Polystyrene is used in a wide range of products including insulation, packaging, and consumer goods. However, polystyrene is quite brittle. Attempts have been made to improve its properties by adding fillers [1, 2], blending it with other polymers [3, 4], grafting it with other polymers [5, 6], or some combination of the above [7, 8]. One important industrial material is high impact polystyrene (HIPS) which is a polystyrene-polybutadiene blend with PS-PB graft copolymers. Studies have shown that the graft linkages are concentrated near the PS-PB interface [5]. In this polymer blend, the rubbery polybutadiene domains act as stress concentrators to induce crazing and absorb energy while the graft linkages provide good interfacial adhesion between the two phases.

In this chapter, polystyrene is blended with various rubber-like polymers and clay nanoparticles (nanoclay). Nanoclay has been shown to be an effective compatibilizer [8, 9, 10]. They can possibly serve as a good alternative to organic linkages (such as graft or block copolymers) because they can be easily melt compounded with the polymers instead of synthesized during a controlled dual polymerization reaction. Rubber-like polymers were chosen to mix with polystyrene and the nanoclay because the elastic nature of the rubbery particles has been shown to be a necessary component of toughened polymer systems.

The polymers blended with polystyrene in this study are polyvinylidene flu-

oride (PVDF), polystyrene-polybutadiene random copolymer (also known as styrene-butadiene-rubber or SBR), and polybutadiene (PB). PVDF is actually a semi-crystalline polymer but was included in this study because upon blending with another polymer, PVDF can break up into very small domains with suppressed crystallinity[9]. Polybutadiene is a component of HIPS and was a natural choice for this study. SBR was included in an attempt to mimic a graft compatibilizer where the styrene component can interact favorably with the matrix while the butadiene component toughens the blend.

Of the polystyrene blends studied, a blend nanocomposite with increased toughness compared to homopolymer polystyrene was found. This blend nanocomposite displays mechanical properties that are comparable to or better than polystyrene blends with grafted copolymers. The studies herein suggest that toughness is related to domain size and that the domain size is controlled by the domain/PS viscosity ratio and the interactions between PS and the domain phase.

5.2 Experimental Part

Characteristics of the polymers used are listed in Table 5.1. Polystyrene pellets and rubber blocks cut down to pellets were ground to 2mm particles. PVDF powder (Kynar 721) was provided by Arkema. Modified montmorillonite clay (Cloisite 20A) was obtained from Southern Clay Products. Both materials were used as received. Cloisite 20A clay (herein referred to as 20A) is modified by dimethyl di-hydrogenated tallow alkylammonium. Polystyrene was combined with the secondary polymer and clay in a speed mixer. For the samples with

Table 5.1: Characteristics of Blend Polymers

Polymer	reference	M_w $\left(\frac{\text{kg}}{\text{mol}}\right)$	Tg (°C)	Source
polystyrene	PS	192	107	Sigma-Aldrich
polybutadiene	PB	175	-93	Lanxess
23% styrene copolymer	mSBR23	130	-48	Michelin
polyvinylidene fluoride	PVDF	215	-38	Arkema

PVDF, the ratio of PVDF:PS:clay was 30:70:5. For the samples with PB or SBR, the ratio was 20:80:5 for rubber:PS:clay. The rubber content was kept low as the extruder is not designed to mix elastomeric materials. The mixture was extruded at 180°C under flowing nitrogen for 5 minutes using a DSM twin screw microcompounder. To mold dog-bone shaped samples (ISO 527-2-5A standard) for tensile testing, a microinjector was used with the barrel at 180°C, the mold at 90°C, and the injection pressure at 110psi.

Blend morphology was examined using a Technai T12 TEM operating at an accelerating voltage of 120kV. Samples for TEM were sectioned from molded dogbones to 70nm at −60°C using a diamond knife. For blends with PVDF, the greater electron density of PVDF domains was sufficient to provide contrast in the TEM. For blends with rubber, the rubber was stained with the vapor of a 4% solution of osmium tetraoxide. The microtomed sections on a copper grid were suspended several millimeters from a droplet of the solution for 40 minutes. Domain size was determined using ImageJ processing program on several images ranging from 2kx to 50kx magnification. Diffraction spectra were collected on a Scintag Inc. $\theta - \theta$ diffractometer with a CuKα source ($\lambda = 1.54$Å) and a germanium detector, scanning at $3°\text{min}^{-1}$. Degree of crystallinity was evaluated by following the equations outlined previously[11, 12] and using a TA instruments Q1000 DSC scanning 10°C/min from ambient temperature to 250°C; a

heat/cool/heat cycle was used to eliminate any thermal history in the extruded material. Mechanical properties were determined using an Instron 5569 tensile tester at an extension rate of 5mm/min (strain rate of 18%/min). Five dogbone specimens were tested for each sample. The standard deviations were within 10% of the average values of the tensile properties. Rheological measurements were made using a MCR 300 under nitrogen flow at 180°C in oscillatory shear configuration with a 1% strain.

5.3 Results

5.3.1 Blends of polystyrene and polyvinylidene fluoride

PVDF and clay as additives have been shown to increase the toughness of a blend as studied in Chapter 4. In that case, clay nanoparticles were able to control the PVDF domain morphology and suppress PVDF crystallinity to aid in toughening the blend. As such, PVDF was studied as a potential toughener for PS. As a matrix phase, PS is different from N6 in that N6 has fairly good mechanical properties to begin with. Regardless, PS-PVDF blend still meets many of the variables that were determined in the previous study to create a good blend. For example, the morphology of a blend nanocomposite is determined by, among other factors, interactions of each polymer with the clay nanoparticles and interactions of the polymers with each other. Previous studies on PS-PVDF blends have shown that while the interaction parameter between PS and PVDF is positive (indicating immiscibility), it is close to zero[13, 14]. As for the added clay compatibilizer, 20A clay is intercalated by both PS and PVDF ho-

mopolymers. 20A is also intercalated when combined in a blend of PS and 30% PVDF (Figure 5.1a). There is little difference among the intercalated samples in terms of d-spacing and order (full width half maximum).

TEM was used to elucidate the blend and blend nanocomposite morphology. Figure 5.2a and figure 5.2b show the PVDF:PS 30:70 blend and blend with 5% 20A clay, respectively. PVDF domain size in the blend is quite varied with a range of 300nm – 4μm. In the blend nanocomposite, there is a greater number of smaller domains, but the size of the small domains are not smaller compared to the small domains in the blend alone. There are also large domains in the nanocomposite, but there are fewer of them and they are smaller than the large domains in the blend alone. The domain size ranges from 300nm – 2μm in the nanocomposite. Figure 5.2c is a higher magnification TEM image of the blend nanocomposite showing the position of the clay layers within the blend. In this figure, the clay resides at the interface of PVDF and PS. Some of the clay layers are within the PVDF domain, and many of the layers reside within the PS matrix. Among other clay stacks, there are some clay stacks that reside only in the PS matrix (not shown). Not all of the domains have clay layers at the PS-PVDF interface.

PVDF is a semi-crystalline polymer, and the presence or absence of crystalline structure in PVDF domains greatly affect blend performance [9]. PVDF crystalline structure in this blend was studied by both XRD and DSC. Figure 5.1b shows the XRD spectra for the blend, blend nanocomposite, homopolymer PVDF, and PVDF nanocomposite. PVDF has two prevalent crystalline phases, α and β, with the α-phase being more thermodynamically stable. In wide angle x-ray, the 001 diffraction pattern for α-phase occurs at $2\theta = 17.2^\circ, 17.9^\circ, 19.5^\circ$

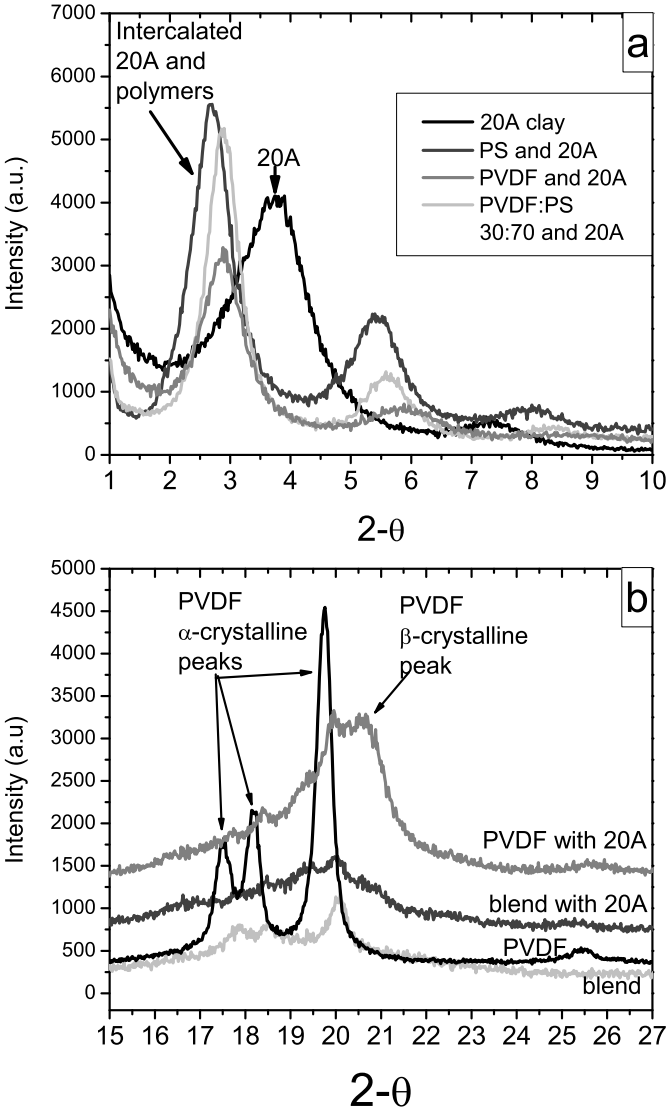

Figure 5.1: X-ray diffraction spectra of a) clay spacing and b) polymer crystallinity in PVDF-PS blends and composites. a) shows that 20A in both PS and PVDF homopolymers is intercalated as well as in PVDF:PS 30:70 blend. b) shows that PVDF homopolymer and the PVDF in PVDF:PS 30:70 blend is mostly α-crystalline form, while PVDF nanocomposite and the PVDF in the blend nanocomposite is a mixture of α and β-crystalline forms.

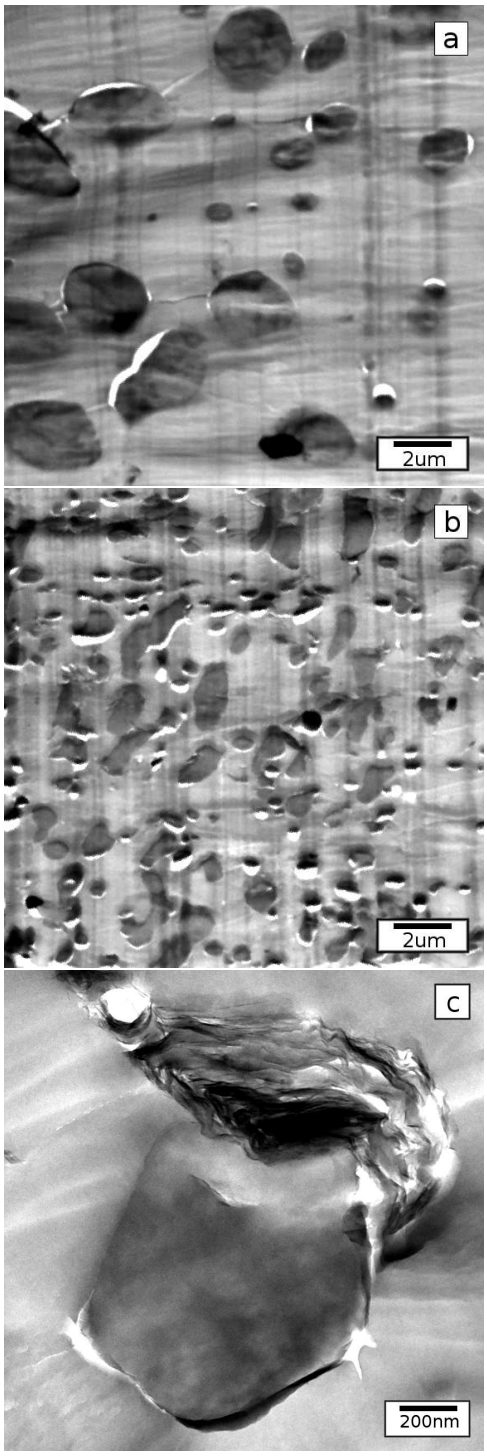

Figure 5.2: TEM images of a) PVDF:PS 30:70 blend, b) blend with 5% 20A clay, and c) blend with clay at higher magnification. PVDF domain size in the blend (a) is quite varied. There is a reduction in domain size for the blend nanocomposite (b), and the domain sizes are not as varied. Clay nanoparticles reside at the PVDF-PS interface (c) as well as in the matrix (not shown). Not all domains contain clay at the surface.

while the peaks for β-phase are at $2\theta = 18.3°, 19.9°$. Homopolymer PVDF exists primarily as the α-phase, but the β-phase, which has been shown to result in a tougher polymer, can be induced with clay nanoparticles [15]. Figure 5.1b shows that homopolymer PVDF contains α-phase crystals, but PVDF-20A nanocomposite contains both α and β-phase crystals. Similarly, PVDF in PVDF:PS 30:70 blend exists in mainly the α-crystalline phase while PVDF in the blend nanocomposite has both crystalline forms. The presence of both crystalline forms confirms that the clay nanoparticles are interacting with the PVDF domains. DSC melting curves of the blend and blend nanocomposite show the same result (Figure 5.3). From the DSC curves, the amount of crystallinity of the PVDF domains was also calculated. The amount of crystallinity of the PVDF in the blend (no clay) is 41%. The PVDF in the blend nanocomposite is slightly more crystalline than the blend with no clay at 45% crystalline. The addition of clay to the blend stabilizes a different PVDF crystalline structure in the blend nanocomposite, and it leaves the amount of crystallinity virtually unchanged.

The reduction in domain sizes and change in PVDF crystalline structure unfortunately does not translate into an improvement in mechanical properties. Figure 5.4 shows a representative stress-strain curve for the blend and blend nanocomposite as well as the homopolymers for comparison. PVDF is softer and less stiff ($E = 1.31 \pm 0.06$GPa) than PS ($E = 2.05 \pm 0.05$GPa), but it is also much more ductile. These properties are generally suited for a domain phase in a toughened system, but in this case, they do not translate to a tougher blend. The PVDF-PS 30:70 blend is slightly less stiff ($E = 1.91 \pm 0.01$GPa) and comparable in strength and ductility compared to PS homopolymer. The addition of PVDF to PS appears to not greatly affect the mechanical properties compared to PS. Comparing the blend to the blend nanocomposite, the blend with clay is

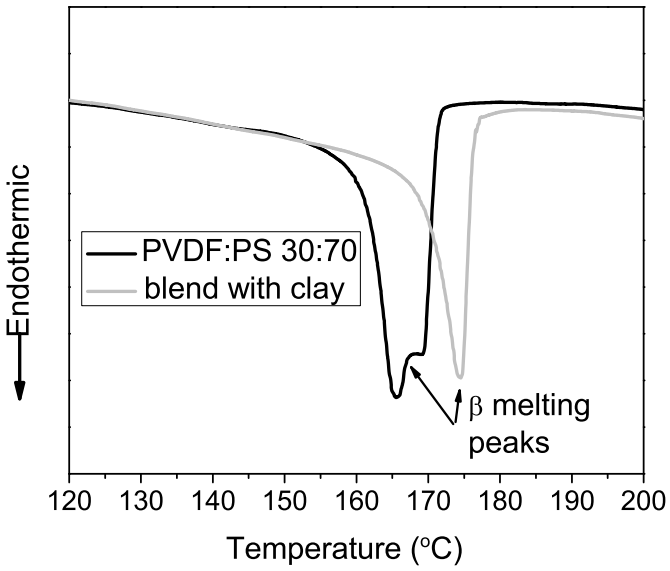

Figure 5.3: DSC melting curves for PVDF:PS 30:70 blend and blend with 5% clay. The melting curve shows that the blend is a mix of α and β-crystalline forms while the blend nanocomposite is mostly β-crystalline forms. The difference between the DSC and XRD results (DSC curves show more β-crystalline form in both the blend and blend nanocomposite) stem from further heat treatments in the DSC.

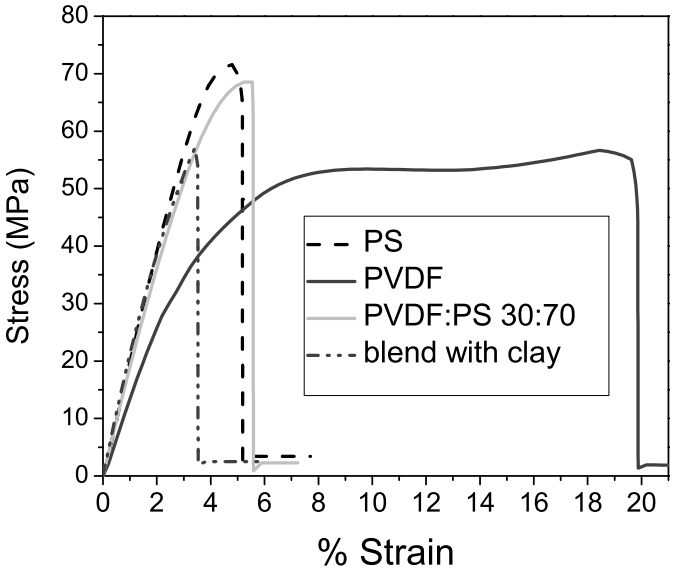

Figure 5.4: Tensile stress-strain curves of PS and PVDF homopolymers, PVDF:PS 30:70 blend, and blend nanocomposite with 20A. PVDF is softer and more ductile than PS but does not significantly affect the mechanical properties of the PVDF:PS 30:70 blend. The blend with clay has slightly worse properties. Regardless both the blend and blend nanocomposite break in brittle fracture.

stiffer (E = 2.18 ± 0.01GPa) compared to blend alone but is also less ductile. All of the samples, however, break in brittle fracture.

5.3.2 Blends of polystyrene and styrene-butadiene-rubber (SBR)

Copolymer domains can provide an advantage over homopolymer domains in that they may contain a component that interacts favorably with the matrix phase, essentially acting as its own compatibilizer. In this section, blends of polystyrene with SBR and clay are studied. With this blend, the copolymer component that interacts favorably with PS is styrene which is chemically identical to the matrix phase. The styrene component in SBR also causes SBR to interact more favorably with clay than homopolymer polybutadiene (as measured by dielectric spectroscopy in Chapter 2), and as determined in Chapter 3, the styrene component in SBR increases clay intercalation kinetics compared to polybutadiene. The clay mixed in the SBR-PS blends, 20A, is the same clay used in the dielectric and kinetic studies. 20A is intercalated both SBR and PS and well as the SBR:PS 20:80 blend (Figure 5.5).

Figure 5.6a and figure 5.6b show SBR:PS 20:80 blend and blend with 5% 20A clay, respectively. SBR domain size in the blend is quite varied with a range of 40nm – 1.3μm. In the blend nanocomposite, the domain size is also quite varied. The small domains in the blend nanocomposite are comparable in size to the small domains of the blend, 40nm. The large domains are only slightly larger at 1.5μm. Figure 5.6c is a higher magnification TEM image of the blend nanocomposite showing the position of the clay layers within the blend. In this

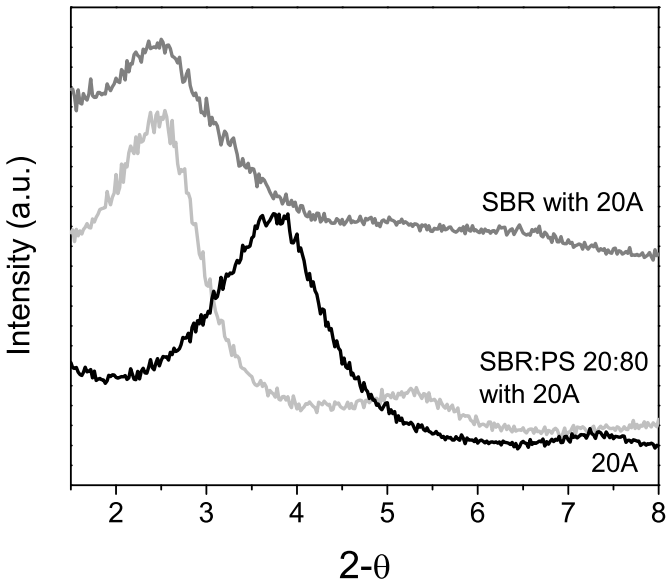

Figure 5.5: XRD diffraction spectra of clay spacing in SBR and SBR-PS blend nanocomposite. 20A is intercalated in both SBR, PS (shown in Figure 5.1), and the SBR:PS blend.

figure, some clay layers reside at the interface of SBR and PS and some clay layers reside in the PS matrix. The layers that do reside at the interface, reside primarily at the interface of medium (100nm) and large sized SBR domains.

Figure 5.7 shows a representative stress-strain curve for the blend and blend nanocomposite as well as PS homopolymer for comparison. The SBR-PS 20:80 blend is less stiff ($E = 1.43 \pm 0.04$GPa) and strong and only slightly more ductile compared to PS ($E = 2.05 \pm 0.05$GPa). The blend nanocomposite is stiffer ($E = 1.53 \pm 0.03$GPa) and 30% more ductile than the blend with no clay. However, despite the increase in ductility, the loss of strength and stiffness of PS due to blending with SBR only make the toughness (defined as the area under the stress-strain curve) of the blend nanocomposite comparable to PS.

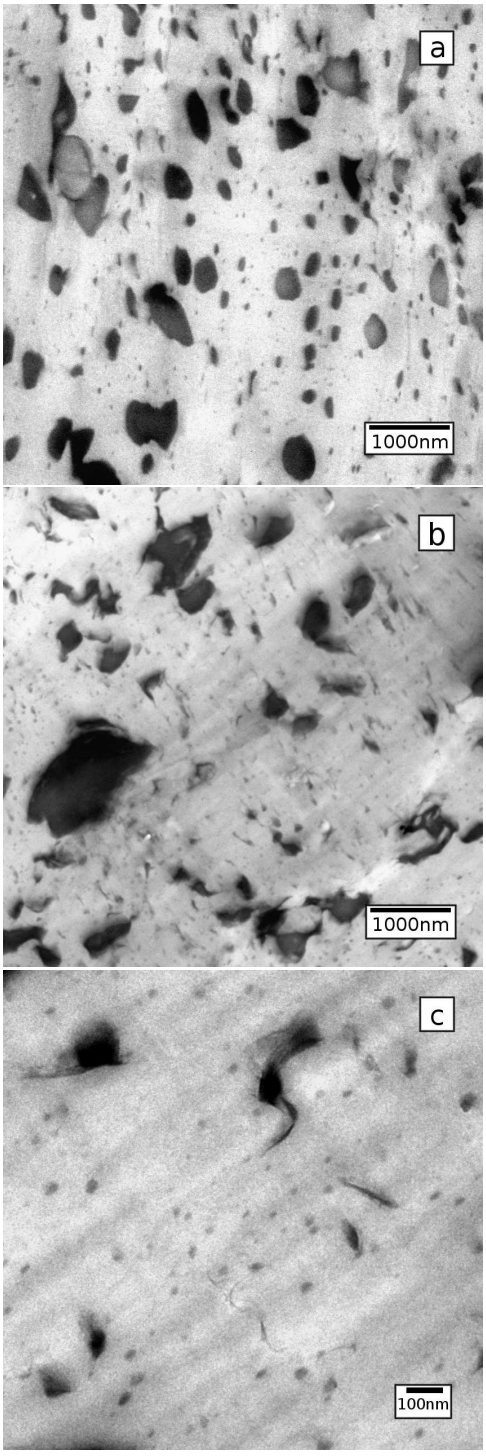

Figure 5.6: TEM images of a) SBR:PS 20:80 blend, b) blend with 5% 20A clay, and c) blend with clay at higher magnification. The domains in both the blend and blend nanocomposite are quite varied. There are slightly larger domains in the blend nanocomposite. Clay nanoparticles reside at the domains and in the matrix. The clay that are at the domains, reside primarily at the larger domains.

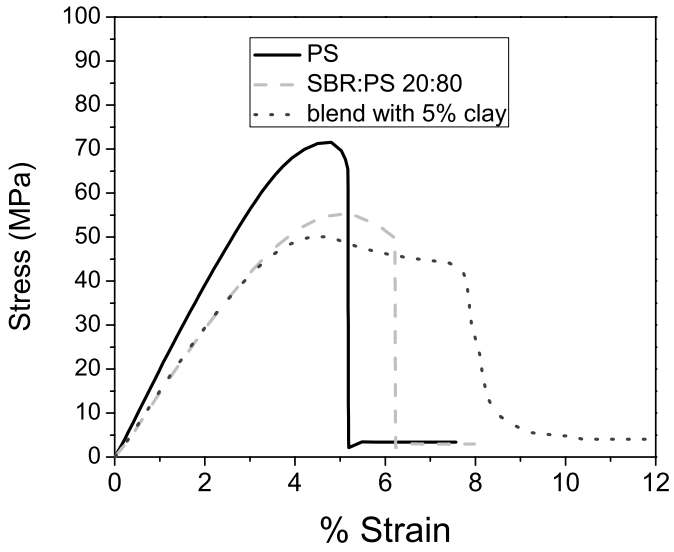

Figure 5.7: Tensile stress-strain curves for PS, SBR:PS 20:80 blend, and blend with 20% clay. The blends are less strong than PS due to the addition of softer PB. The blend nanocomposite is slightly more ductile than the blend. However, despite the increases in ductility, the loss in strength (compared to PS), only make toughness of the blend nanocomposite comparable to PS.

5.3.3 Blends of polystyrene and polybutadiene

In industry, polybutadiene is the polymer of choice to toughen polystyrene, often by way of grafting to polystyrene and creating a commercial blend known as high impact polystyrene or HIPS. In this section, a melt mixed blend of polystyrene, polybutadiene, and clay is studied. This blend is different from the blend studied in the previous section in that there is no styrene component in the domain phase with which to potentially interact with homopolymer polystyrene or the clay. The clay used in the PB-PS blends, 20A, is the same as for the SBR and PVDF blends. 20A is intercalated by PS, as established in Section 5.3.1, and it is also intercalated by PB and PB-PS 20:80 blend (Figure 5.8).

Figure 5.9a and figure 5.9b show PB:PS 20:80 blend and blend with 5% 20A

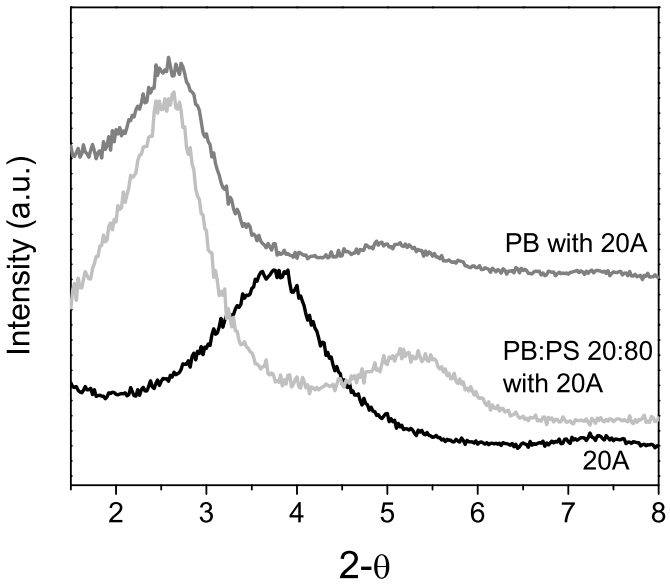

Figure 5.8: XRD diffraction spectra of clay spacing in PB and PB-PS blend nanocomposite. 20A is intercalated in both PB, PS (shown in Figure 5.1), and the PB:PS blend.

clay, respectively. PB domain size in the blend is quite small and fairly uniform with an average size of 70nm. In the blend nanocomposite, the domain size is more varied. There are the same 70nm sized domains that were present in the blend, but there are also larger domains approximately 200nm in size. The clay layers are located both at the PB-PS interface and in the PS matrix. The layers that do reside at the interface, reside primarily at the interface of larger PB domains.

Figure 5.10 shows a representative stress-strain curve for the blend and blend nanocomposite as well as PS homopolymer for comparison. The PB-PS 20:80 blend is less stiff (E = 1.20 ± 0.02GPa) and strong but much more ductile compared to PS which is to be expected given that the blend contains 20% PB. When clay is added to the blend, there is a decrease in ductility compared to the blend with no clay, but the blend nanocomposite is still 3 times as ductile as the homopolymer PS. The clay also increases the stiffness and strength of the blend

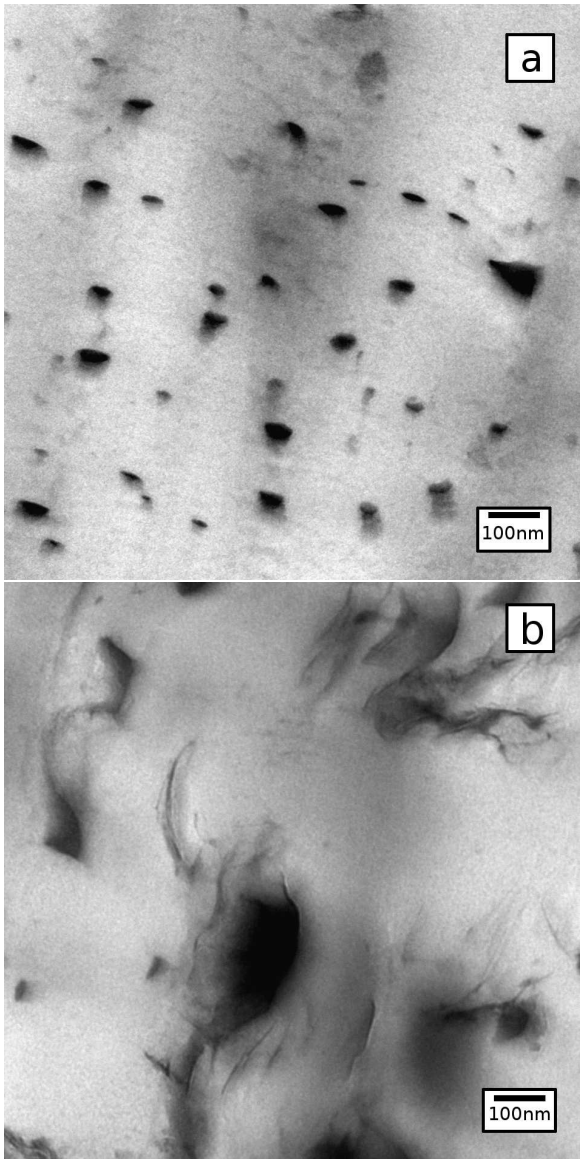

Figure 5.9: TEM images of a)PB:PS 20:80 blend and b)blend with 5% 20A clay. The domains in the blend are very small and uniform in size. The domain size in the blend nanocomposite is more varied. Clay nanoparticles appear to be in the matrix and at the interface of the larger domains.

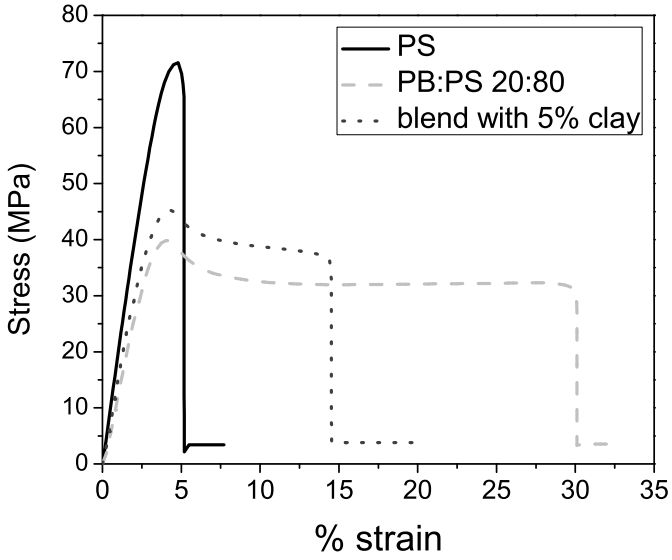

Figure 5.10: Tensile stress-strain curves for PS, PB:PS 20:80 blend, and blend with 5% 20A clay. The blends are less strong than PS but also much more ductile. The blend nanocomposite is less ductile than the blend but still 3 times as ductile as PS.

nanocomposite (E = 1.41 ± 0.05GPa) compared to the blend with no clay.

5.4 Discussion

The blend and blend nanocomposite that showed the greatest improvements in toughness compared to polystyrene are the blends with polybutadiene. Not only were the mechanical properties of these blends the best in this study, they are comparable or better than high impact polystyrene (HIPS). Table 5.2 compares the mechanical properties of the blend and blend nanocomposite prepared in this study with commercially available HIPS and PB-PS blend with graft copolymer previously reported in the literature. The blend nanocomposite is significantly stronger (1.5 to 3 times as strong) than the blends with grafting, comparable in stiffness (especially given that the blend studied here contains

Table 5.2: Mechanical properties of PB:PS blend, blend with clay, [a]commercially available HIPS[16], and [b]synthesized PB-PS graft polymer[5]

sample	rubber phase weight %	Modulus (GPa)	Tensile strength (MPa)	Elongation %
PB:PS blend	20	1.20	40	33
blend with clay	19	1.41	45	16
HIPS 1[a]	8	1.56	14	43
HIPS 2[a]	6	1.82	29	31
PB-PS graft[b]	21	1.52	18.4	20

twice the amount of rubber content of HIPS), and comparable in elongation compared to the lab prepared graft polymer (although less ductile compared to the commercial HIPS). Polybutadiene has always been the polymer of choice for toughening polystyrene[16, 5, 3], but in this case, polystyrene was toughened through the process of melt blending the two polymers with nanoclay not *in-situ* graft polymerization.

Just as for the PVDF-N6 blends in Chapter 4, there appears to be a direct link between mechanical toughening and the domain phase; tougher blends have smaller, more uniform domains that are elastomeric with no additional microstructure. The toughest blend was PB-PS. Polybutadiene domains do not contain crystalline structures like PVDF or multiple interacting components like SBR. Polybutadiene also forms the smallest domains in the polystyrene matrix. The blend itself (no clay) is actually tougher than the blend nanocomposite due to higher ductility. The blend is more ductile because the PB domains in the blend are smaller and more uniform in size compared to the domains in the blend nanocomposite, and smaller domains and domain size distribution are generally associated with tougher blends [9, 17].

Adding clay to the PB-PS blend aided domain coalescence resulting in a less ductile blend nanocomposite compared to the blend alone. One possible reason

for the coalescence of larger domains in the blend nanocomposite might be the relative changes in viscosity ratio. Recall from Chapter 4, that the two main factors controlling domain size in a blend is the ratio of the viscosity of the domain phase to the viscosity of the matrix phase and interfacial tension between the domain and matrix phase. For small domains, a viscosity ratio close to unity and a small interfacial tension are required. Based on rheological studies, the viscosities of PS and PB at 180°C and $10s^{-1}$ shear rate are $3900Pa * s$ [18] and $3500Pa * s$ [3], respectively. Thus for the blend, the viscosity ratio is close to unity and the domain sizes are small. Generally, when clay is added to a polymer, the viscosity of the polymer increases. When clay is added to the blend, it is likely that the viscosity of the matrix phase increases relative to viscosity of the domain phase (as clay is dispersed in the matrix more than in the domains). The increased viscosity of the matrix phase skews the viscosity ratio away from unity, and as this effect seems to outweigh the reduction in interfacial tension, the domains in the nanocomposite are larger than in the blend. However, the loss in ductility due to larger domains in the blend nanocomposite is not detrimental. The blend nanocomposite is still 3 times as ductile as homopolymer polystyrene and is comparable in ductility to PB-PS grafting methods. In addition, the clay reinforces the blend so it is actually stronger than commercial HIPS.

The SBR-PS nanocomposite blend contains four interacting components compared to the three interacting components of PB-PS nanocomposite blend (polystyrene, polybutadiene, and clay). The four interacting variables in SBR-PS nanocomposite are homopolymer polystyrene, styrene component of SBR, butadiene component of SBR, and clay. While additional interactions can be beneficial to a polymer blend, it can also lead to a complicated blend morphol-

ogy. This is observed in the TEM images of the blend and blend with clay. The domains in both the blend and the blend nanocomposite are quite varied in size (with approximately the same domain size range). The combination of large domain sizes and wide domain size distribution resulted in a blend with no improvements in toughness compared to homopolymer polystyrene.

In the case of PVDF-PS blend, the domain size of the blend nanocomposite is smaller compared to the blend alone. It is likely that the reduction in domain size is due to the viscosity ratio effect, but in the opposite direction as PB-PS. Based on rheological studies, the viscosities of PS and PVDF at 180°C and $10s^{-1}$ shear rate are $3900Pa * s$ [18] and $5150Pa * s$, respectively. These viscosities are dissimilar to each other, and thus the domain size of the PVDF-PS blend is large. When clay is added, it increases the viscosity of the matrix phase (PS). With the viscosity of PS increased, the viscosity ratio is skewed closer to unity, and the domain size of the blend nanocomposite is smaller than of the blend alone.

Unfortunately this reduction and stabilization of domain sizes did not translate to improved mechanical properties because the microstructure of the domain phase is also crucial to mechanical response. Even though the domain size was reduced in the blend nanocomposite, the domains remained very crystalline. In order for PVDF to be effective in blend toughening, the PVDF crystallinity needs to be suppressed as evidenced in Chapter 4. For PVDF domain crystallinity suppression the domain size needs to be on the order of 50nm. The domain size in PVDF-PS blend nanocomposite is 300nm. The viscosity ratio has already been harnessed to some extent to reduce domain sizes. The other way to reduce domain sizes is through a reduction in interfacial tension, but this is a large hurdle for PVDF-PS blends. PVDF and N6, while immiscible, in-

teract favorably with each other. The solubility parameters for PVDF and N6 are $11.3\left(\frac{\text{cal}}{\text{cm}^3}\right)^{0.5}$ [19] and $11.6\left(\frac{\text{cal}}{\text{cm}^3}\right)^{0.5}$ [20], respectively. The closer the solubility parameters of two polymers, the more favorably they interact. The solubility parameter of PS on the other hand is $9.1\left(\frac{\text{cal}}{\text{cm}^3}\right)^{0.5}$ [20]. Given the polymer-polymer interaction, it is unlikely that PVDF domains in PS can be reduced to the same level as the domains in N6, and thus PVDF is not a suitable toughening agent for PS.

The challenge in creating a toughened polystyrene blend by melt mixing is controlling the domain size so that the domains are small and uniform in size. Domain morphology, and thus mechanical properties, is controlled both kinetically and thermodynamically. Domain size is determined kinetically through the viscosity ratio of domain phase to matrix phase. Thermodynamically, the domain morphology is controlled through the interactions of the blend components. Ideally both factors play a role to minimize domain size and maximize blend mechanical properties.

BIBLIOGRAPHY

[1] Hasegawa, N.; Okamoto, H.; Kawasumi, M.; Usuki, A. *J. Appl. Polym. Sci.* **1999**, *74*, 3359–3364.

[2] Chang, T.; Kisliuk, A.; Rhodes, S.; Brittain, W.; Sokolov, A. *Polymer* **2006**, *47*, 7740–7746.

[3] Joseph, S.; Thomas, S. *Eur. Polym. J.* **2003**, *39*, 115–125.

[4] Ansari, M.; Haghtalab, A.; Semsarzadeh, M. *Rheol. Acta.* **2006**, *45*, 983–993.

[5] Sardelis, K.; Michels, J.; Allen, G. *Polymer* **1987**, *28*, 244–250.

[6] Dorazio, L.; Guarino, R.; Mancarella, C.; Martuscelli, E.; Cecchin, G. *J. Appl. Polym. Sci.* **1997**, *65*, 1539–1553.

[7] Si, M.; Araki, T.; Ade, H.; Kilcoyne, A.; Fisher, R.; Sokolov, J.; Rafailovich, M. *Macromolecules* **2006**, *39*, 4793–4801.

[8] Ray, S.; Pouliot, S.; Bousmina, M.; Utracki, L. *Polymer* **2004**, *45*, 8403–8413.

[9] Vo, L.; Giannelis, E. *Macromolecules* **2007**, *40*, 8271–8276.

[10] Chow, W.; Ishak, Z.; Ishiaku, U.; Karger-Kocsis, J.; Apostolov, A. *J. Appl. Poly. Sci.* **2004**, *91*, 175–189.

[11] Tjong, S.; Bao, S. *J. Polym. Sci. Part B: Polym. Phys.* **2004**, *42*, 2878–2891.

[12] Priya, L.; Jog, J. *J. Polym. Sci. Part B: Polym. Phys.* **2002**, *40*, 1682–1689.

[13] Del Rio, C.; Acosta, J. *Eur. Polym. J.* **1995**, *31*, 581–587.

[14] Del Rio, C.; Acosta, J. *Eur. Polym. J.* **1996**, *32*, 913–917.

[15] Shah, D.; Maiti, P.; Gunn, E.; Schmidt, D.; Jiang, D.; Batt, C.; Giannelis, E. *Adv. Mater.* **2004**, *16*, 1173–1177.

[16] Rios-Guerrero, L.; Keskkula, H.; Paul, D. *Polymer* **2000**, *41*, 5415–5421.

[17] Kudva, R.; Keskkula, H.; Paul, D. *Polymer* **2000**, *41*, 225–237.

[18] Lobe, V.; White, J. *Poly. Eng. Sci.* **1979**, *19*, 617–624.

[19] Bottino, A.; Capannelli, G.; Munari, S.; Turturro, A. *J. Polym. Sci. Part B: Polym. Phys.* **1988**, *26*, 785–794.

[20] Jang, B.; Wang, D.; Wilkie, C. *Macromolecules* **2005**, *38*, 6533–6543.